



HAL
open science

Sources of dissolved iron to oxygen minimum zone waters on the Senegalese continental margin in the tropical North Atlantic Ocean: Insights from iron isotopes

Jessica K Klar, C. Schlosser, J. A. Milton, E. M. S. Woodward, F. Lacan, I. J. Parkinson, E. P. Achterberg, R.H. James

► To cite this version:

Jessica K Klar, C. Schlosser, J. A. Milton, E. M. S. Woodward, F. Lacan, et al.. Sources of dissolved iron to oxygen minimum zone waters on the Senegalese continental margin in the tropical North Atlantic Ocean: Insights from iron isotopes. *Geochimica et Cosmochimica Acta*, 2018, 236, pp.60-78. 10.1016/j.gca.2018.02.031 . hal-03771965

HAL Id: hal-03771965

<https://hal.science/hal-03771965v1>

Submitted on 7 Sep 2022

HAL is a multi-disciplinary open access archive for the deposit and dissemination of scientific research documents, whether they are published or not. The documents may come from teaching and research institutions in France or abroad, or from public or private research centers.

L'archive ouverte pluridisciplinaire **HAL**, est destinée au dépôt et à la diffusion de documents scientifiques de niveau recherche, publiés ou non, émanant des établissements d'enseignement et de recherche français ou étrangers, des laboratoires publics ou privés.

1 Sources of dissolved iron to oxygen minimum zone waters 2 on the Senegalese continental margin in the tropical North 3 Atlantic Ocean: Insights from iron isotopes

4 JK Klar^{1,2}, C Schlosser³, JA Milton¹, EMS Woodward⁴, F Lacan², IJ Parkinson⁵, EP Achterberg^{1,3}, RH
5 James¹

6 (1) Ocean and Earth Science, National Oceanography Centre, University of Southampton, European Way, Southampton SO14 3ZH, UK

7 (2) LEGOS, Université de Toulouse, CNES, CNRS, IRD, UPS, 14 Avenue Edouard Belin, 31400 Toulouse, France

8 (3) GEOMAR Helmholtz Centre for Ocean Research, Wischhofstraße 1-3, 24148 Kiel, Germany

9 (4) Plymouth Marine Laboratory, Prospect Place, The Hoe, Plymouth PL1 3DH, UK

10 (5) School of Earth Sciences, University of Bristol, Queens Road, Bristol, BS8 1RJ, UK

11 **Keywords:** tropical Atlantic Ocean; iron isotopes; oxygen minimum zone; benthic iron;
12 remineralisation; dissolved aluminium; dust; GEOTRACES

13 Abstract

14 Oxygen minimum zones (OMZs) cover extensive areas of eastern boundary ocean regions and play an
15 important role in the cycling of the essential micronutrient iron (Fe). The isotopic composition of
16 dissolved Fe (dFe) in shelf and slope waters on the Senegalese margin was determined to investigate
17 the processes leading to enhanced dFe concentrations (up to 2 nM) in this tropical North Atlantic
18 OMZ. Our results show that benthic sources of Fe inputs, characterised by low $\delta^{56}\text{Fe}$ down to -0.33
19 ‰, are upwelled to surface waters and recycled in the water column by remineralisation processes.
20 We show that regeneration of sinking organic material becomes a more important dFe source with
21 distance from the shelf and this remineralised dFe has relatively high $\delta^{56}\text{Fe}$ values (up to +0.41 ‰).
22 Remineralisation plays an important role in the redistribution of dFe that is mainly supplied by
23 benthic and atmospheric inputs, although dust loading, calculated from dissolved aluminium
24 concentrations, was low at the time of our study (0.17 to 0.7 $\mu\text{mol dFe m}^{-2} \text{d}^{-1}$). As OMZs are
25 expected to expand, our data provide important insights into Fe sources and Fe cycling in the tropical
26 North Atlantic Ocean.

27 1. Introduction

28 Iron (Fe) is an essential element for marine phytoplankton (Martin, 1990; Martin and Fitzwater,
29 1988), including nitrogen fixing diazotrophs (e.g., Berman-Frank et al., 2001; Falkowski, 1997). Iron
30 supply therefore influences the nitrogen cycle (Schlosser et al., 2014) and the strength of the

31 biological carbon pump (Coale et al., 2004). Marine photosynthesis is responsible for about half of
32 the global atmospheric CO₂ uptake (Le Quéré et al., 2013), and phytoplankton growth is limited by Fe
33 availability in ~ 50 % of the world's ocean (Moore et al., 2001). Proper constraints on the sources of
34 Fe to the oceans, and the processes that regulate its distribution, are essential for global models that
35 are used to calculate past and future climate scenarios (e.g., Boyd and Ellwood, 2010).

36 The supply of Fe to the oceans is temporally and spatially variable. The low solubility of Fe in
37 oxygenated seawater (pH ~8.1) (Liu and Millero, 2002), its highly particle reactive nature (Goldberg,
38 1954) and its uptake by marine microorganisms (Coale et al., 2004) lead to rapid removal of Fe from
39 the surface ocean. Therefore, Fe concentrations tend to be highest close to source regions. Iron is
40 mainly delivered to the ocean from atmospheric dust deposition, margin sediments, rivers,
41 groundwater discharge and hydrothermal vents (Boyd and Ellwood, 2010, and references therein).

42 In the open ocean dissolved Fe (dFe; i.e. filterable through 0.4 or 0.2 µm) concentrations typically
43 range between <0.2 to ~1 nmol L⁻¹ (e.g., Klunder et al., 2012; Klunder et al., 2011; Nishioka and
44 Obata, 2017; Resing et al., 2015; Rijkenberg et al., 2014) and are generally lowest in the surface
45 ocean. However, dFe concentrations of 1 to 1.7 nmol L⁻¹ have been observed within oxygen minimum
46 zones (OMZs) (Conway and John, 2014; Fitzsimmons et al., 2013; John et al., 2017; Milne et al., 2017;
47 Rijkenberg et al., 2012; Ussher et al., 2013; Ussher et al., 2010). Elevated biological production in
48 surface waters caused by upwelling of nutrient rich waters in eastern boundary ocean regions results
49 in the development of OMZs through enhanced oxygen consumption associated with sinking organic
50 matter degradation (Karstensen et al., 2008). OMZs usually extend between ~100 and ~700 m water
51 depth in regions with sluggish circulation and reduced ventilation, such as the eastern tropical
52 Atlantic and eastern tropical Pacific (Stramma et al., 2005). Elevated dFe concentrations encountered
53 in OMZs are attributed to remineralisation of biogenic Fe that sinks from the surface (Fitzsimmons et
54 al., 2013; Rijkenberg et al., 2012), and transport of high dFe – low oxygen waters from the adjacent
55 continental shelf forms another source (Conway and John, 2014; Ussher et al., 2010). In addition,
56 elevated dFe concentrations off the Peru margin of the eastern tropical South Pacific have been
57 attributed to reversible scavenging of dFe from sinking particles (John et al., 2017). The relative
58 importance of each of these processes for Fe supply to oxygen deficient waters is, however, poorly
59 constrained. As anthropogenic climate change results in the expansion and intensification of OMZs in
60 the worlds' oceans (Brandt et al., 2010; Schmidtko et al., 2017; Stramma et al., 2008b) and is
61 postulated to have important effects on the biogeochemical cycling of many redox-sensitive
62 elements, including Fe, as well as ecosystem functioning (Chan et al., 2008; Keeling et al., 2010), the
63 Fe sources to OMZs need to be constrained.

64 Iron isotopes (expressed in delta notation of the $^{56}\text{Fe}/^{54}\text{Fe}$ ratio of the sample relative to that of the
65 reference material IRMM-014) are a relatively new tool that can help to identify Fe supply and
66 removal mechanisms in the ocean as well as biogeochemical processing of Fe within the ocean (e.g.
67 (Lacan et al., 2008), that cannot be provided by concentration data only. The isotopic signatures of
68 dFe for different sources are distinct. The continental crust has an average $\delta^{56}\text{Fe}$ value of $+0.09 \pm 0.10$
69 ‰ (2 SD, $n = 46$; Beard et al. (2003)). The $\delta^{56}\text{Fe}$ value of atmospheric dust in the North Atlantic
70 ($\sim +0.07 \pm 0.11$ ‰; Mead et al., 2013; Waeles et al., 2007) is similar to the crustal value, but is
71 modified during delivery and dissolution in surface seawater, leading to a $\delta^{56}\text{Fe}$ signature of between
72 $+0.3$ and $+0.7$ ‰ (Conway and John, 2014), although this value may be the result of other processes,
73 such as biological uptake. Fe reduction in anoxic sediments and the efflux of pore waters supply
74 isotopically light Fe to the overlying water column, leading to typical $\delta^{56}\text{Fe}$ values in oxygenated
75 bottom waters of between -1.25 and -0.1 ‰ (Chever et al., 2015; Conway and John, 2014; Klar et al.,
76 2017a), and as low as -3.5 ‰ in anoxic bottom waters (John et al., 2012). In contrast, non-reductive
77 dissolution of lithogenic material on continental margins and in the water column is thought to lead
78 to a $\delta^{56}\text{Fe}$ of dFe between -0.3 and $+0.5$ ‰ (Abadie et al., 2017; Homoky et al., 2013; Radic et al.,
79 2011), and an isotopic difference between dissolved and particulate Fe ($\Delta^{56}\text{Fe}_{\text{dFe-pFe}}$) of $+0.27 \pm 0.25$
80 ‰ (Labatut et al., 2014). The isotopic signal of river-derived dFe is $+0.3$ to $+0.4$ ‰, and is not altered
81 during estuarine mixing with adjacent coastal waters (Bergquist and Boyle, 2006; Escoube et al.,
82 2009; Poitrasson et al., 2014). The $\delta^{56}\text{Fe}$ values of all of these sources can nevertheless be modified
83 by chemical and physical transformations within the ocean.

84 Upon delivery of Fe to the ocean from reducing sediments, rivers or hydrothermal vents, the change
85 in ambient temperature, salinity, oxygen concentrations, pH and redox potential leads to Fe
86 precipitation into mineral phases, such as Fe-(oxy)hydroxides and Fe-sulphides. The remaining
87 reduced Fe (Fe(II)) after partial oxidation to Fe(III) followed by Fe(III)-(oxy)hydroxide precipitation
88 could theoretically be up to 3.9 ‰ lighter than the initial Fe(II) pool (Klar et al., 2017b). The
89 formation of iron sulphide (FeS) minerals leads to an isotopic fractionation of $\Delta^{56}\text{Fe}_{\text{Fe(II)-FeS}} < +0.77$ ‰
90 (Rouxel et al., 2008). It is now clear that dFe is rapidly complexed to organic ligands upon delivery to
91 the ocean, with >99 % of dFe bound to organic ligands (Gledhill and Buck, 2012) and references
92 therein). Ligand complexed Fe has $\delta^{56}\text{Fe}$ values up to 0.6 ‰ higher than inorganic dFe (Dideriksen et
93 al., 2008; Morgan et al., 2010). In the presence of sufficient light and macronutrients, Fe is rapidly
94 taken up by primary production in the surface ocean. Opposing directions of Fe isotopic fractionation
95 associated with biological uptake have been reported. The uptake of isotopically light Fe with an
96 isotopic difference between the particulate and dissolved $\delta^{56}\text{Fe}$ values, $\Delta^{56}\text{Fe}_{\text{pFe-dFe}} < -0.54$ ‰ has
97 been observed in the waters east of New Zealand and in the equatorial Pacific Ocean (Ellwood et al.,

98 2015; Radic et al., 2011). In contrast, relatively low $\delta^{56}\text{Fe}$ values of dFe (-0.01 ‰) were observed in
99 the deep fluorescence maximum and dFe minimum in the North Atlantic Ocean (Conway and John,
100 2014). Thus, it appears that the sinking of dead phytoplankton cells and its remineralisation at depth
101 can lead to the release of both isotopically light (Ellwood et al., 2015; Radic et al., 2011) or heavy
102 (Conway and John, 2014) Fe to the dissolved pool. Iron is highly particle reactive (Goldberg, 1954),
103 and it is thought that adsorption/desorption of Fe onto/from particle surfaces is continuously
104 occurring throughout the water column (Milne et al., 2017). The effects of scavenging/desorption
105 on the isotopic composition of dFe are not yet clear. While one study found that scavenging resulted
106 in the preferential uptake of heavy Fe onto particles ($\Delta^{56}\text{Fe}_{\text{dFe-scavFe}} = -0.67$ ‰; Ellwood et al., 2015),
107 results from another study indicated differences in $\delta^{56}\text{Fe}$ values of scavenged Fe relative to dFe were
108 small ($\Delta^{56}\text{Fe}_{\text{dFe-scavFe}} = +0.3 \pm 0.3$ ‰; Radic et al., 2011).

109 To constrain the processes that regulate the behaviour of Fe within OMZs, we have determined the
110 isotopic signature of dFe in the West African shelf and slope region of the tropical North Atlantic
111 Ocean. We use our data to identify the sources of dFe in the OMZ and assess the effects of internal
112 processes, such as Fe-ligand formation, biological uptake, remineralisation and scavenging, as well as
113 water mass transport and mixing on the distribution of Fe. This work contributes to the international
114 GEOTRACES program (www.geotraces.org).

115 2. Materials and methods

116 2.1 Cleaning procedures

117 Seawater samples were collected in one litre high density polyethylene (HDPE) bottles (Nalgene),
118 which were acid cleaned following a three-step procedure. Firstly, the bottles were filled and
119 submerged for at least 3 days in 2 % Decon. After a thorough rinse in reverse osmosis water, the
120 bottles were filled and submerged in a 6 M hydrochloric acid (HCl, analytical grade, Fisher Scientific)
121 bath for one week. The bottles were then rinsed with purified deionised water (Milli-Q, Merk
122 Millipore; resistivity = 18.2 M Ω cm) and transferred into a 7 M nitric acid (HNO₃, analytical grade,
123 Fisher Scientific) bath for another week. Finally, the bottles were thoroughly rinsed with purified
124 deionised water, double bagged and stored in boxes until sampling on the ship.

125 Laboratory equipment used for sample processing was mainly polytetrafluoroethylene (PTFE)
126 fluorinated ethylene propylene (FEP) or perfluoroalkoxy (PFA), with some low density polyethylene
127 (LDPE) and polyethylene (PE) components, cleaned thoroughly in dilute HCl and HNO₃ before and
128 between uses.

129 2.2 Sample collection

130 Samples were collected during RRS *Discovery* cruise D361 (GEOTRACES section GA06) between 7th
131 February and 19th March 2011. Water was collected from four stations, ranging from 51 to 2656 m
132 water depth (Figure 1), using a trace metal clean conductivity-temperature-pressure (CTD) rosette
133 system. The trace metal clean CTD (TM-CTD) rosette was equipped with 24 10 L OTE (Ocean Test
134 Equipment, Inc.) bottles (with external springs, modified for trace metal work) that were mounted
135 onto a titanium frame. The CTD was deployed on a non-conducting Kevlar wire fitted with a Seabird
136 auto-fire module that triggered the OTE bottles at pre-programmed depths. Sampling depths were
137 selected according to salinity, temperature, dissolved oxygen concentration and transmission
138 profiles, obtained immediately beforehand by a standard stainless steel CTD deployment.
139 Immediately after recovery of the trace metal clean CTD rosette, the OTE bottles were transferred
140 into a trace metal clean container for sub-sampling.

141 Water samples from the TM-CTD were filtered through 0.2 μm Acropak 500 filter capsules (Pall
142 Corp.), that were pre-rinsed with ~ 5 L surface seawater from the trace metal clean ‘tow-fish’, or
143 through acid cleaned 0.45 μm polyethersulfone membrane filters (Supor, Pall Gelman). The filters
144 were rinsed with several 100 mL of sample, followed by three rinses of the HDPE sample bottle
145 before filling up. For Fe isotopes, three 1 L bottles were filled for each sample. Filtration was carried
146 out under oxygen-free N_2 gas with a low overpressure of 10-50 kPa.

147 Surface seawater samples were collected with the trace metal clean ‘tow-fish’, deployed on the side
148 of the ship. Seawater was pumped into the clean laboratory using a trace metal clean Teflon
149 diaphragm pump through acid washed braided PVC tubing during the ships transit (10 knots).
150 Samples were filtered in-line through a 0.8/0.2 μm cartridge filter (AcroPak1000) into acid-washed
151 low-density polyethylene bottles for dFe and dAl analysis.

152 Samples were acidified to pH ~ 2 with concentrated HCl (Romil, Ultra Purity Acid, UpA). Isotope
153 samples were double bagged and stored for shipping back to the National Oceanography Centre
154 (NOC) in Southampton for analysis. Dissolved Al samples were allowed to equilibrate for at least 24 h
155 prior analysis on board.

156 2.3 Analysis of dissolved Fe Isotopes and Fe concentrations

157 Iron for isotope analysis was preconcentrated using a nitriloacetic acid (NTA) Superflow resin
158 (Qiagen) and purified by anion exchange chromatography (BioRad AG1-x8 resin). Two
159 preconcentration protocols were used, a batch method, modified from (John and Adkins, 2010) and a
160 column method, based on (Lacan et al., 2010). The average yield from both methods was $95 \pm 8\%$ Fe
161 ($n = 15$) and the procedure blank was 1.7 ± 0.5 ng Fe ($n=11$) for the batch method and 2.3 ± 0.7 ng Fe

162 (n=10) for the column method. Sample volumes ranged from 1 to 3 L with 100 to 350 ng Fe. When
163 dFe concentrations were $< 1.5 \text{ nmol L}^{-1}$, individual 1 L bottles were combined in LDPE cubitainers to
164 increase the sample volume. Dissolved Fe concentrations were analysed on board using
165 chemiluminescence flow-injection-analysis following a method outlined by Klunder et al. (2011) and
166 are published in Schlosser et al. (2014) and Milne et al. (2017).

167 Isotopic measurements of samples were carried out in duplicate on a multi-collector inductively
168 coupled plasma mass spectrometer (MC-ICP-MS) (Thermo Fisher Neptune) at the University of
169 Southampton. Instrumental mass bias was corrected by addition of a double spike (45.7% ^{57}Fe , 53.1
170 % ^{58}Fe and 0.5 % ^{54}Fe) prior to sample processing and $^{56}\text{Fe}/^{54}\text{Fe}$ sample ratios are expressed as $\delta^{56}\text{Fe}$
171 relative to the average $^{56}\text{Fe}/^{54}\text{Fe}$ value for the Fe isotope reference material IRMM-014 (Institute for
172 Reference Materials and Measurements) determined during the same analytical session. The
173 external precision and accuracy of the isotope measurements was assessed by multiple analyses of
174 an Fe isotope standard during each analytical session. The average value of ETH (Eidgenössische
175 Technische Hochschule, Zürich) hematite standard for all analytical sessions was $0.52 \pm 0.07 \text{ ‰}$ (2 SD,
176 $n = 54$). This value compares well with previous measurements of the ETH hematite standard
177 reported in (Lacan et al., 2010) ($0.52 \pm 0.08 \text{ ‰}$, 2 SD, $n = 81$). Analytical replicates, which consisted of
178 splitting the sample and replicating the entire analytical procedure, yielded $2\text{SD} < 0.08 \text{ ‰}$ for samples
179 6_16 and 8_13 (Table 1).

180 We have further validated our Fe isotope method by blind analysis of two seawater samples that had
181 already been analysed in F. Lacan's lab (LEGOS, Toulouse, France). The seawater samples were
182 collected from Station 14 during Cruise R/V Kilo Moana 06252006 and Fe isotope results obtained at
183 LEGOS are published in Radic et al. (2011). Fe concentrations were sub nano-molar, which is
184 characteristic of open ocean seawater. We obtained $\delta^{56}\text{Fe}$ values of $+0.07 \pm 0.07 \text{ ‰}$ ($n = 2$) for
185 sample 14-2 at 849 m depth (vs. $+0.22 \pm 0.05 \text{ ‰}$ in Radic et al., 2011) and $+0.34 \pm 0.06 \text{ ‰}$ ($n = 2$) for
186 sample 14-6 at 198 m depth (vs $+0.40 \pm 0.06 \text{ ‰}$ in Radic et al., 2011). These replicate analyses are
187 within the range of inter-lab reproducibility ($\pm 0.17 \text{ ‰}$) at 0.4 nmol L^{-1} , reported in Boyle et al. (2012).

188 2.4 Analysis of dissolved aluminium concentrations

189 Dissolved aluminium (dAl) concentrations were determined on board by flow injection analysis using
190 a lumogallion-Al fluorescence technique originally developed by Resing and Measures (1994) and
191 modified according to Brown and Bruland (2008). The analytical procedure was validated by
192 analysing North Atlantic GEOTRACES Reference Seawater. GD-23 yielded $18.2 \pm 1.0 \text{ nmol kg}^{-1} \text{ dAl}$, $n =$
193 4 (vs a consensus value of $17.7 \pm 0.2 \text{ nmol kg}^{-1}$) and GS-57 yielded $27.1 \pm 1.1 \text{ nmol kg}^{-1} \text{ dAl}$, $n = 5$ (vs a
194 consensus value of $27.5 \pm 0.2 \text{ nmol kg}^{-1}$).

195 2.5 Auxiliary data

196 Salinity (conductivity), temperature, depth (pressure) and oxygen concentrations in the water
197 column were determined using a Seabird CTD sensor mounted on the rosette frame. Sensors were
198 cross-calibrated with discrete seawater analyses using the Winkler method for oxygen and
199 conductivity measurements of a certified reference material for salinity. Chlorophyll-a content was
200 monitored using a fluorometer fitted on the rosette frame and calibrated against analyses of discrete
201 samples collected from standard CTD casts and the underway tow fish.

202 Concentrations of seawater nitrate, nitrite, silicate, ammonium and phosphate were determined on
203 board the RRS *Discovery*, using a 5-channel segmented flow auto-analyser (Bran and Luebbe AAIII)
204 (Woodward and Rees, 2001).

205 3. Results

206 3.1 Hydrography and oxygen content

207 Off the coast of Senegal, four main water masses were identified from potential temperature, salinity
208 and potential density data (Figure 2). The surface 40 m consisted of Tropical Surface Water (TSW; σ_θ
209 $< 25.8 \text{ kg m}^{-3}$) (Stramma et al., 2008a; Stramma et al., 2005). Between the isopycnals (σ_θ) 25.8 and
210 27.1 kg m^{-3} , at temperatures above 8°C , subsurface waters down to 500 m depth mainly consisted of
211 South Atlantic Central Water (SACW) (Stramma et al., 2005). SACW is formed from Indian Ocean
212 Central Water, which is transferred to the Atlantic Ocean by the Agulhas and Benguela currents
213 (Stramma and England, 1999). After flowing northwards with the Benguela Current, SACW flows
214 westward to the tropical Atlantic with the South Equatorial Current (SEC) (Stramma and Schott,
215 1999). Below 500 m water depth, northward flowing Antarctic Intermediate Water (AAIW) was
216 identified by a pronounced salinity minimum at ~ 34.8 PSU, elevated oxygen and nutrient
217 concentrations, and was observed at stations 2 and 3 with its core at 900 m depth (Stramma et al.,
218 2005). Southward flowing North Atlantic Deep Water (NADW) was observed below 1200 m depth to
219 the seafloor at Station 2 ($\sigma_\theta > 27.6 \text{ kg m}^{-3}$), and is characterised by its relatively high salinity (Stramma
220 and England, 1999).

221 The flow field in the upper 800 m of the northeastern subtropical Atlantic is controlled by a wind
222 driven subtropical gyre (Stramma et al., 2005) (Figure 1). Upwelling occurs near the coast of Senegal
223 and Mauritania, as well as in the Guinea Dome (Schott et al., 2004). Coastal upwelling replaces the
224 water moved offshore by Ekman transport, driven by equatorward winds (Stramma et al., 2005).
225 Upwelling in the Guinea Dome is due to cyclonic circulation, associated with the North Equatorial
226 Counter Current (NECC), the northern NECC (nNECC) and the North Equatorial Undercurrent (NEUC)

227 (Stramma et al., 2008a; Stramma et al., 2005) (Figure 1). The Guinea Dome and its related circulation
228 are weakened during the winter, even though they exist throughout the year (Siedler et al., 1987).

229 In the upper 40 m of the water column, oxygen concentrations were $> 200 \mu\text{mol kg}^{-1}$. Oxygen
230 concentrations were $< 70 \mu\text{mol kg}^{-1}$ at depths between ~ 40 and ~ 900 m (the approximate extension
231 of these waters at 400 m depth is shown in Figure 1). Oxygen depleted waters roughly coincided with
232 the extension of SACW and the upper part of AAIW (Figure 2). Oxygen concentrations reached a
233 minimum of $\sim 45 \mu\text{mol kg}^{-1}$ at around 400 m depth at Stations 2 and 3. NADW was well oxygenated,
234 and oxygen concentrations were $> 200 \mu\text{mol kg}^{-1}$ near the seafloor. Our observations agree with
235 previous reports of oxygen concentrations $> 35 \mu\text{mol kg}^{-1}$ for the OMZ in the tropical North Atlantic
236 Ocean, compared to concentrations within the OMZ of the eastern tropical Pacific Ocean being < 3
237 $\mu\text{mol kg}^{-1}$ (Stramma et al., 2008b). The OMZ in the tropical North Atlantic Ocean consists of poorly
238 ventilated upwelled waters, flowing westward from the African coast. The OMZ is contained by
239 ventilation from below by AAIW; in the north and south by the eastward flowing zonal jets; and in
240 the west by subtropical gyre waters (Stramma et al., 2005).

241 3.2 Distributions of dFe, $\delta^{56}\text{Fe}$ and macronutrients

242 Dissolved Fe concentrations in the water column ranged between 1.33 nmol L^{-1} and 6.3 nmol L^{-1}
243 (Figure 4 and Table 1). On the shelf, the highest dFe concentrations were observed near the seafloor
244 and lowest concentrations in the surface waters, indicating benthic supply. By contrast, the slope
245 stations (2 and 3) showed a mid-depth maximum between 300 m and 1100 m (up to 3.77 nmol L^{-1})
246 and rather similar dFe concentrations above and below ($\sim 1.5 \text{ nmol L}^{-1}$) of this feature. Dissolved Fe
247 showed an approximately linear relationship with nitrate and phosphate (Figure 3). The slope of the
248 regression line was steeper for the offshore stations 2 and 3 than for the two shelf stations 4 and 5.

249 $\delta^{56}\text{Fe}$ values for dFe ranged between -0.33 and $+0.41 \text{ ‰}$ (Figure 4 and Table 1). $\delta^{56}\text{Fe}$ values were
250 lowest over the shelf ($\sim -0.3 \text{ ‰}$) close to the seafloor, and increased towards the crustal value ($+0.09$
251 $\pm 0.10 \text{ ‰}$, 2 SD; Beard et al., 2003) higher up in the water column (Figure 4 and Table 1).

252 On the slope, Station 3 (1041 m water depth) displayed lowest $\delta^{56}\text{Fe}$ values (between -0.27 and -0.15
253 ‰) in oxygen depleted waters. Higher $\delta^{56}\text{Fe}$ values are observed at 200 m ($+0.06 \text{ ‰}$) and 600 m
254 depth (-0.08 ‰). The highest $\delta^{56}\text{Fe}$ values (-0.06 to $+0.41 \text{ ‰}$) were observed at the furthest offshore
255 Station 2 (2656 m water depth). Here, $\delta^{56}\text{Fe}$ values increased from -0.06 ‰ at 200 m depth to $+0.41$
256 ‰ at 500 m depth. Between 600 m and the seafloor, there was little variation in $\delta^{56}\text{Fe}$, with values
257 around $+0.1 \text{ ‰}$.

258 4. Discussion

259 4.1 Benthic supply of dFe

260 It is now clear, however, that shelf sediments are a source of dFe to overlying seawater even if this
261 water is oxygen replete (Klar et al., 2017a; Mackey et al., 2002; Marsay et al., 2014; Planquette et al.,
262 2007). Thus, the consideration of benthic Fe supply to seawater in biogeochemical models leads to
263 an improved reproduction of dFe distributions (Siedlecki et al., 2012; Tagliabue et al., 2017). The
264 release of dFe from seafloor sediments can be broadly classified into two categories: (i) dissimilatory
265 iron reduction and (ii) non-reductive dissolution.

266 Dissimilatory iron reduction (DIR) occurs in anoxic sediments and results in the release of soluble
267 Fe(II) into pore waters (e.g., (Severmann et al., 2006), yielding high Fe(II) concentrations in the
268 millimolar range, characterised by a light isotopic signature (-2 to -1 ‰) (Henkel et al., 2016; Homoky
269 et al., 2009; Klar et al., 2017a; Severmann et al., 2006). Upward diffusion of Fe(II) into oxygenated
270 pore waters or overlying bottom water is readily oxidised to Fe(III) (Millero et al., 1987), which forms
271 insoluble amorphous Fe-(oxy)hydroxide minerals at seawater pH (Liu and Millero, 2002; Ussher et al.,
272 2004). It has been observed that as Fe(III) is removed from pore waters, the remaining pore water Fe
273 isotopic composition shifts towards lower values (i.e., $\delta^{56}\text{Fe}$ down to -3.5 ‰; Severmann et al., 2010).
274 This is in agreement with experimental observations, that have shown that equilibrium fractionation
275 between Fe(II) and Fe(III) results in the $\delta^{56}\text{Fe}$ value of aqueous Fe(III) being up to 3.5 ‰ greater than
276 that of the coexisting aqueous Fe(II) (e.g., Welch et al., 2003), hence, the $\delta^{56}\text{Fe}$ value of dFe depends
277 on the proportion of Fe(III) removed from the dissolved phase (Klar et al., 2017b).

278 On the other hand, non-reductive dissolution (NRD) of lithogenic material leads to the release of dFe
279 with heavier isotopic compositions ($\Delta^{56}\text{Fe}_{\text{dFe-pFe}} = +0.20 \pm 0.11$ ‰; Radic et al., 2011), resulting in
280 observed average $\delta^{56}\text{Fe}$ values of +0.22 ‰ in oxic sediment pore waters (Homoky et al., 2013) and
281 +0.37 ‰ in seawater (Radic et al., 2011). However, benthic Fe fluxes associated with NRD are
282 significantly lower (0.11 to $0.23 \mu\text{mol Fe m}^{-2} \text{d}^{-1}$; Homoky et al., 2013) than those associated with
283 reductive dissolution in low bottom-water oxygen environments (400 to $866 \mu\text{mol Fe m}^{-2} \text{d}^{-1}$; Noffke
284 et al., 2012; Severmann et al., 2010).

285 On the Senegalese shelf, elevated dFe concentrations (up to 6.35 nmol L^{-1}) close to the seafloor are
286 thus indicative of a sedimentary Fe source to the overlying waters. Benthic inputs to the West African
287 margin were also observed on the Mauritanian shelf, at $\sim 18^\circ\text{N}$, where diffusive Fe(II) fluxes from
288 shelf sediments (<200 m depth) to bottom waters with $<50 \mu\text{mol kg}^{-1}$ oxygen, determined from pore
289 water Fe concentrations, were between 10 and $30 \mu\text{mol m}^{-2} \text{d}^{-1}$ (Lomnitz, 2017). These fluxes were
290 somewhat lower than fluxes observed on the Californian shelf (<10 to $>300 \mu\text{mol m}^{-2} \text{d}^{-1}$) using

291 benthic chambers (Severmann et al., 2010). Maximum pore water Fe concentrations were
292 considerably lower (up to $20 \mu\text{mol L}^{-1}$) on the Mauritanian shelf than on the Californian margin (up to
293 $300 \mu\text{mol L}^{-1}$), indicating that Fe fluxes supplied from sediments are lower on the West African shelf.

294 Shelf stations 4 and 5 were characterised by low $\delta^{56}\text{Fe}$ values (down to -0.33‰) in low oxygen
295 waters ($\sim 50 - 100 \mu\text{mol kg}^{-1}$) close to the seafloor (Figure 4). Note that no samples were collected
296 within 50 m of the seafloor at Station 5, so even lower $\delta^{56}\text{Fe}$ and O_2 values may have been found
297 there. Previous studies (e.g., John et al., 2012; Klar et al., 2017a) have shown that low $\delta^{56}\text{Fe}$ values
298 indicate pore water Fe(II) efflux to bottom waters. However, even lower $\delta^{56}\text{Fe}$ values (e.g., down to $-$
299 3.45‰ ; John et al., 2012) than those reported here have been observed in bottom waters overlying
300 highly reducing margins. Hence, the isotopic composition observed in bottom waters of our study
301 area may reflect the presence of a NRD component. Reported NRD fluxes from marine sediments are
302 insignificant compared to fluxes from DIR. However, reported fluxes from NRD are from regions with
303 a low supply of lithogenic material (low atmospheric dust depositions). Due to high atmospheric dust
304 fluxes to our study area, the NRD component may be more significant, and, hence, potentially makes
305 an important contribution to the entire benthic dFe flux. Other processes that could also explain the
306 relatively high bottom water $\delta^{56}\text{Fe}$ values are explored below.

307 As a result of the progressive removal of Fe(III)-(oxy)hydroxides towards the sediment-water
308 interface, sediment porewaters generally show lowest isotopic compositions closest to the surface
309 (down to -3.5‰ ; Severmann et al., 2010). If we were to expect a similar process to occur across the
310 sediment-water interface, even lower $\delta^{56}\text{Fe}$ values should be observed in bottom waters on the
311 Senegalese margin. However, the relatively higher $\delta^{56}\text{Fe}$ values in bottom waters (-0.33‰), suggest
312 that the isotopic composition has been modified during transport across the sediment-seawater
313 interface. Organic ligands most likely favour the heavy Fe isotopes, with the $\delta^{56}\text{Fe}$ of ligand bound Fe
314 being up to 0.6‰ higher than that of the inorganic Fe fraction (Dideriksen et al., 2008; Morgan et al.,
315 2010). The stabilisation of Fe in bottom waters by ligand complexation could partly prevent
316 precipitation of Fe(III)-(oxy)hydroxides, facilitating the transport of pore water Fe into overlying
317 bottom waters (Hioki et al., 2014; Jones et al., 2011). We therefore suggest that some part of the
318 pore water dFe is complexed with organic ligands, which may also be supplied to sediment pore
319 waters during the degradation of organic material. Dissolved Fe stabilisation due to the complexation
320 to organic ligands at the sediment-water interface has also been suggested in previous studies (e.g.
321 (Klar et al., 2017a), where elevated Fe(II) concentrations were observed in oxic bottom waters over
322 the shelf for longer time periods than predicted, and Fe isotopic signals shifted from as low as -3‰
323 in pore waters to up to -0.1‰ in bottom waters. Organic complexation of benthic Fe at the
324 sediment-water interface combined with a NRD component could explain the shift towards higher

325 $\delta^{56}\text{Fe}$ values (down to -0.3 ‰) compared to values reported for pore waters elsewhere (as low as ~ -
326 3.5 ‰; e.g., Severmann et al., 2010; Klar et al., 2017a).

327 In contrast to the shallow coastal stations, bottom waters at slope Station 3 were more oxygenated
328 (up to $140 \mu\text{mol kg}^{-1}$), but had similar $\delta^{56}\text{Fe}$ values (~ -0.3 ‰), suggesting a similar Fe supply
329 mechanism than on the shelf. However, bottom water dFe concentrations (up to 2.9 nmol L^{-1}) were
330 significantly lower at Station 3 compared to stations 4 and 5. Hence, benthic inputs occurred on the
331 slope at Station 3, but were weaker than on the shelf. Elevated dFe concentrations and the benthic
332 Fe isotopic signature (<-0.2 ‰) also persisted ~ 800 m above the seafloor in low oxygen waters at
333 Station 3 (Figure 4), which could be due to upwelling, that is usually high at this time of year (Schott
334 et al., 2004). This is confirmed by the upwards vertical flux of dFe at the bottom of the surface mixed
335 layer at Station 3, that was $0.024 \mu\text{mol m}^{-2} \text{ d}^{-1}$ at the time of our study (Milne et al., 2017).

336 In addition to Fe-ligand complexation, the transport of dFe from sediment pore waters towards the
337 overlying bottom waters and vertical/horizontal transport away from bottom waters may have also
338 been facilitated by low oxygen concentrations ($> 45 \mu\text{mol kg}^{-1}$; Figure 4) through impediment of Fe(II)
339 removal. Here we assume that sediments are a source of reduced Fe. Although we have no
340 measurements of Fe(II) in our samples, Pacific Ocean waters with oxygen concentrations down to 50
341 $\mu\text{mol kg}^{-1}$, contained Fe(II) representing up to 20 % of the dFe pool (Chever et al., 2015). The Fe(II)
342 half-life ($t_{1/2}$) in bottom waters at station 4 and 5 was estimated to be ~ 30 to 70 min (using equations
343 from Millero *et al.*, 1987, and $[\text{O}_2] = 79$ to $93 \mu\text{mol kg}^{-1}$, $T = 16$ to $17 \text{ }^\circ\text{C}$, $\text{Sal} = 35.62$ to 35.67 , $\text{pH} = 7.75$
344 to 7.80). Theoretical oxidation rates were slower in bottom waters at Station 3, with Fe(II) $t_{1/2} \sim 325$
345 min ($[\text{O}_2] = 130 \mu\text{mol kg}^{-1}$, $T = 5.4 \text{ }^\circ\text{C}$, $\text{Sal} = 34.84$, $\text{pH} = 7.81$). Longer Fe(II) $t_{1/2}$ at this station may have
346 maintained the relatively high dFe concentrations supplied by sediment pore waters, and perhaps
347 partly prevented the formation of Fe-(oxy)hydroxides. Relatively high dFe concentrations within the
348 OMZ on the slope also suggest that longer Fe(II) $t_{1/2}$ may have an effect on the transport of dFe away
349 from bottom waters. However, isotopic compositions characteristic of benthic inputs (<-0.20 ‰ from
350 400 to 900 m depth) are only observed in the OMZ at Station 3 and not at Station 2 (Figure 4). These
351 findings will be discussed in more detail in Section 4.5.

352 Negative seawater $\delta^{56}\text{Fe}$ values attributed to the release of Fe(II) from anoxic sediments into the
353 overlying water column have also been observed in an anoxic basin off the coast of southern
354 California (John et al., 2012). Dissolved Fe concentrations were as high as 29 nmol L^{-1} , $\delta^{56}\text{Fe}$ values in
355 bottom waters were as low as -3.45 ‰, and bottom water oxygen concentrations were $< 5 \mu\text{mol kg}^{-1}$.
356 At oxygen concentrations similar to those found within the OMZ in our study (~ 50 to $75 \mu\text{mol kg}^{-1}$),
357 dFe in their study ranged from 2.4 to 4.3 nmol L^{-1} and $\delta^{56}\text{Fe}$ ranged from -1.13 to -0.8 ‰ off the

358 Californian coast. This suggests that benthic fluxes of dFe are greater in the southern California basin
359 than on the West African margin. In addition, bottom waters in the Peru upwelling area had $\delta^{56}\text{Fe}$
360 values as low as -1.25 ‰, associated with O_2 concentrations of $< 35 \mu\text{mol kg}^{-1}$ (Chever et al., 2015;
361 John et al., 2017). These results are in agreement to our findings, considering that the OMZ in the
362 equatorial Pacific Ocean has lower oxygen concentrations than the OMZ in the tropical Atlantic
363 (Stramma et al., 2008b). In addition, Chever et al. (2015) have demonstrated that the dFe pool
364 reflects the isotopic composition of the ferrous Fe, which is presumably released from the sediments.
365 Interestingly, the $\delta^{56}\text{Fe}$ values of bottom waters on the West African margin were similar to those
366 found in bottom waters of an oxic temperate shelf (-1.0 to -0.1 ‰; Klar et al., 2017a).

367 Furthermore, our results agree well to low $\delta^{56}\text{Fe}$ values of down to -0.5 ‰ in the eastern tropical
368 North Atlantic Ocean north of Cape Verde Islands, which were also attributed to Fe released from
369 reducing sediments into a water column with oxygen levels $>220 \mu\text{mol kg}^{-1}$ (Conway and John, 2014).
370 In their study, the shallowest station close to the African shelf was ~ 3000 m deep, hence lacking
371 $\delta^{56}\text{Fe}$ values on the continental slope and shelf that may have provided further evidence for tracing
372 benthic Fe released into the water column. Our stations, located $\sim 6^\circ$ to the south of the stations
373 shown in Conway and John (2014) complement this coastal gap of $\delta^{56}\text{Fe}$ values. Conway and John
374 (2014) attributed the end-member $\delta^{56}\text{Fe}$ value of -2.4 ‰ (observed on the Californian margin, John
375 et al., 2012) to the reducing benthic Fe source from the eastern margin for calculating its
376 contribution to their ocean transect. However, our study suggests that the end-member $\delta^{56}\text{Fe}$ value
377 of the reducing benthic Fe source may be closer to -0.3 ‰ on the eastern tropical North Atlantic
378 margin, which would allow for a better constrained estimation of its inputs to the ocean.
379 Nevertheless, we also advise that mass-balance calculations using Fe isotopes should be used with
380 caution due to the reactive nature of Fe in seawater, which is mostly associated with isotopic
381 fractionation.

382 The eastern tropical Atlantic is characterised by relatively high upwelling rates (e.g., Ussher et al.,
383 2013), and therefore high dFe bottom waters are most likely transported towards surface waters,
384 especially on the shelf. Shelf and slope waters loaded with dFe were most likely advected along
385 isopycnals towards the open ocean due to the westward direction of the main currents in this area.
386 This is confirmed by net upwards vertical fluxes below the surface mixed layer and net offshore
387 horizontal fluxes that were calculated in our study area (Milne et al., 2017). Horizontal dFe fluxes
388 were highest on the shelf ($5185 \mu\text{mol m}^{-2} \text{d}^{-1}$) and decreased with distance from the coast (down to
389 $21.5 \mu\text{mol m}^{-2} \text{d}^{-1}$ at Station 2; Milne et al., 2017). Vertical upward dFe fluxes were also highest on the
390 shelf ($16 \mu\text{mol m}^{-2} \text{d}^{-1}$ vs 0.024 to 0.043 on the slope).

391 4.2 Atmospheric supply of Fe to the surface ocean

392 The study area is located in close proximity to the Sahara and Sahel deserts, which deliver large
393 amounts of dust to the North Atlantic Ocean (Jickells et al., 2005; Kramer et al., 2004; Patey et al.,
394 2015). Dissolved aluminium (dAl) is a near conservative tracer of lithogenic material in seawater
395 (Measures and Brown, 1996), as it is only removed by scavenging processes (Moran and Moore,
396 1992) with minor incorporation into siliceous frustules (Gehlen et al., 2002). Assuming that dAl in the
397 surface mixed layer is entirely supplied by atmospheric dust, that dust is composed of 8.2 % w/w Al
398 and 5.6 % w/w Fe (Taylor, 1964), and that both elements are dissolved in the same proportion, dust
399 supplied dFe can be calculated (Table 2). Accordingly, 60 % of dFe in the surface mixed layer is
400 provided by dust on the shelf and 50 to 155 % on the slope. Some part of the Fe supplied to the
401 surface mixed layer may have been taken up by phytoplankton or scavenged onto sinking particles.
402 This may explain why we observe lower dFe concentrations at Station 3 than calculated from dAl
403 concentrations. At the other stations, the excess dFe may have been supplied from shelf sediments
404 and were upwelled. Assuming that the residence time of dAl is 1.2 ± 0.5 years in tropical Atlantic
405 waters (Dammshäuser et al., 2011), and that 4 ± 2 % of Saharan dust is dissolved in seawater (Buck et
406 al., 2010), the aerosol dFe flux is estimated to be $0.17 \pm 0.14 \mu\text{mol m}^{-2} \text{d}^{-1}$ on the shelf and $0.20 - 0.71$
407 $\mu\text{mol m}^{-2} \text{d}^{-1}$ on the slope (Table 2).

408 This compares well with direct aerosol measurements and soluble aerosol Fe flux estimates
409 performed during the same cruise. The soluble Fe flux from aerosols was $0.075 \mu\text{mol m}^{-2} \text{d}^{-1}$ on the
410 shelf (Stations 4 and 5) and $0.074 \mu\text{mol m}^{-2} \text{d}^{-1}$ on the slope, compared to $0.135 \mu\text{mol m}^{-2} \text{d}^{-1}$ in the
411 open ocean at 12 °N (Milne et al., 2017). Slight differences between the methods are expected, as
412 aerosol fluxes derived from dAl measurements in surface waters represent average fluxes over ~ 1.2
413 years. It should be noted that the aerosol flux calculation from Al is linked to major caveats and
414 assumptions. Al is highly particle reactive and, hence, its concentration in surface waters is most
415 likely influenced by particle loading (Figure 4). Therefore, the aerosol fluxes calculated from dAl
416 concentrations are highly dependent on Al residence times, which are controlled by particle
417 scavenging. Aerosol fluxes can be as high as $74 \mu\text{mol Fe m}^{-2} \text{d}^{-1}$ on the West African margin during
418 dust storms (Croot et al., 2004). Hence, atmospheric depositions were relatively low but significant in
419 our study area at the time of sampling.

420 We have no $\delta^{56}\text{Fe}$ measurements from within the surface mixed layer (SML, 11 to 19 m thick) and
421 dFe isotopic compositions are likely significantly modified below the SML due to scavenging and
422 remineralisation processes. Hence, we are not able to assess the isotopic composition of dust-
423 derived dFe in our study area. However, surface waters at 25 m depth on the shelf were
424 characterised by higher $\delta^{56}\text{Fe}$ values (-0.11 to $+0.03$ ‰), and lower dFe concentrations (up to 3 nmol

425 L⁻¹), compared to bottom waters (Figure 4). The shift towards higher isotopic values from 40 towards
426 25 m depth is indicative of dust-derived dFe to the surface ocean. NRD of sinking lithogenic material
427 leads to the release of dFe with high $\delta^{56}\text{Fe}$ values $+0.27 \pm 0.25$ ‰ higher (Labatut et al., 2014) than
428 that of the lithogenic material ($\delta^{56}\text{Fe} \sim +0.07 \pm 0.11$ ‰; Mead et al., 2013; Waeles et al., 2007).
429 Hence, NRD may explain the relatively high $\delta^{56}\text{Fe}$ values throughout the water column on the shelf.
430 In the North Atlantic Ocean, north of Cape Verde islands, high $\delta^{56}\text{Fe}$ values of +0.3 to +0.7 ‰ in the
431 surface mixed layer were attributed to a strong atmospheric dust supply (Conway and John, 2014).
432 The high $\delta^{56}\text{Fe}$ values of the aerosol signal in seawater, relative to that of atmospheric dust ($\delta^{56}\text{Fe} \sim$
433 $+0.07 \pm 0.11$ ‰; Mead et al., 2013; Waeles et al., 2007) was attributed to the formation of strong Fe-
434 ligand complexes during dust dissolution, which preferentially incorporate the heavier Fe isotopes
435 ($\Delta^{56}\text{Fe}_{\text{LFe-dFe}} = 0.6$ ‰; (Dideriksen et al., 2008; Morgan et al., 2010). To properly assess the effects of
436 atmospheric deposition on the isotopic composition of dFe in seawater, we are lacking isotopic
437 measurements of aerosols in the study area and of particulate material in the water column.

438 4.3 Fe Isotopic fractionation by biogeochemical processes

439 Concentrations of chlorophyll-a indicated that levels of biological activity in the surface waters were
440 high, with levels up to $\sim 1.5 \mu\text{g L}^{-1}$ on the shelf and up to $2 \mu\text{g L}^{-1}$ on the slope (Figure 4). Maximum
441 Chl-a and lowest transmittance were immediately below the surface layer (0 to 15 m depth) and thus
442 above the shallowest Fe isotopes sample. It is important to note that significant changes in $\delta^{56}\text{Fe}$
443 values linked to high biological activity are expected in surface waters. Uptake of isotopically light Fe
444 linked to biological activity has previously been observed ($\Delta^{56}\text{Fe}_{\text{PFe-DFe}} < -0.54$ ‰; Ellwood et al., 2015;
445 Radic et al., 2011). By contrast, (Conway and John, 2014) record relatively light $\delta^{56}\text{Fe}$ values of dFe
446 (e.g., -0.01 ‰ vs $+0.20$ ‰ above and below) associated with the deep fluorescence maximum (136
447 m) in the North Atlantic Ocean. John et al. (2017) observed a decrease in $\delta^{56}\text{Fe}$ of dFe in the upper
448 few hundred metres and suggested this to be due to biological uptake, however, this was not
449 observed in all their profiles. The direction of Fe isotopic fractionation could depend on
450 phytoplankton type.

451 Even though we were not able to assess the isotopic fractionation of Fe associated with biological
452 uptake directly, we were able to do this indirectly by investigating remineralisation of sinking organic
453 material throughout the water column. Remineralisation of sinking organic material plays an
454 important role in recycling Fe in the ocean (e.g., Fitzsimmons et al., 2013; Rijkenberg et al., 2012).
455 The amount of remineralised dFe in the water column was calculated from apparent oxygen
456 utilisation (AOU), assuming an AOU/C ratio of 1.6 (Martin et al., 1987) and a Fe/C ratio of $15 \mu\text{mol}$
457 Fe/mol C, measured in phytoplankton cells on the west African margin (Twining et al., 2015) (Figure
458 5). This ratio is similar to that estimated in the eastern tropical North Atlantic during cruise AMT15

459 (13 $\mu\text{mol Fe/mol C}$; Ussher et al. (2013)). These calculations suggest that on the shelf, 25 to 40 % of
460 dFe was provided by remineralisation of sinking organic material. The rest must have been supplied
461 by another source, most likely sediments. On the slope at Station 2, remineralisation was the
462 dominant dFe source, especially within the OMZ (between 40 and 900 m depth), and partly
463 represented > 100 % dFe, which suggests that part of the remineralised dFe had been rapidly
464 removed by scavenging processes.

465 Higher levels of remineralisation were associated with the release of relatively heavy Fe isotopes
466 (Figure 5). It has been shown that remineralisation of organic material is less effective in OMZs
467 (Cavan et al., 2017), and therefore, it is not certain if the high $\delta^{56}\text{Fe}$ values are reflecting the
468 remineralisation of the entire biogenic Fe pool or that of an unknown fraction. Other processes such
469 as adsorption/desorption of Fe onto/from particles and dissolution of lithogenic particles could
470 overprint $\delta^{56}\text{Fe}$ values throughout the water column, however, we suggest that these changes are
471 relatively small. At Station 3, highest remineralisation extents at 600 m depth (Figure 5) coincided
472 with a $\delta^{56}\text{Fe}$ value of -0.08 ‰. At Station 2, the proportion of dFe supplied by remineralisation was
473 consistently highest within the OMZ and was correlated to high $\delta^{56}\text{Fe}$ values (+0.02 to +0.41 ‰).
474 Highest remineralisation proportions at Station 2 coincided with a $\delta^{56}\text{Fe}$ value of +0.41 ‰ at 500 m
475 depth, the highest $\delta^{56}\text{Fe}$ value measured in this study. Interestingly, these relatively high isotopic
476 values were associated with a decrease in dFe concentrations at both stations, suggesting rapid
477 scavenging onto particles. Therefore, scavenging of dFe onto particles could also explain the heavy
478 isotopic compositions. Our results suggest biological uptake of heavy dFe isotopes in surface waters,
479 followed by release of heavy dFe isotopes during remineralisation of this material as it sinks
480 throughout the water column followed by rapid scavenging of some part of the remineralised dFe
481 onto sinking particles. Our results contradict previous studies, which suggested that biological Fe
482 uptake incorporates the lighter isotopes (Ellwood et al., 2015; Radic et al., 2011). However, our
483 results are consistent with the findings in Conway et al (2014), where isotopically light dFe was
484 associated with the deep fluorescence maxima and the dFe concentration minima in the North
485 Atlantic.

486 The nearly constant dFe concentrations (1.3 to 1.7 nmol L^{-1}) below 1400 m depth at Station 2,
487 associated with constant $\delta^{56}\text{Fe}$ values ($\sim+0.1$ ‰) may be the result of a dynamic exchange of Fe
488 between the dissolved and particulate phases (Homoky et al., 2012; John and Adkins, 2012; Labatut
489 et al., 2014; Milne et al., 2017). The combination of the different processes involving particles, that
490 include scavenging of Fe onto particles, desorption and non-reductive dissolution from sinking
491 lithogenic particles, potentially leads to dFe isotopic fractionation observed (Abadie et al., 2017;
492 Ellwood et al., 2015; John and Adkins, 2012; John et al., 2017).

493 **4.4 Isotopic signatures within water masses**

494 Between 700 and 1100 m water depth, AAIW was present at stations 2 and 3. The $\delta^{56}\text{Fe}$ values in this
495 water mass were $\sim +0.1\text{‰}$ ($n = 3$) at Station 2 and -0.30 to -0.08‰ ($n = 4$) at Station 3. AAIW was
496 located immediately over the seafloor at Station 3, with enhanced dFe concentrations and low $\delta^{56}\text{Fe}$
497 values indicating a relatively strong supply of benthic dFe to bottom waters, overwriting the isotopic
498 signature of AAIW. In previous studies, it has been observed that AAIW transports isotopically light
499 Fe (-0.37 to -0.17‰) within southern hemisphere basins of the Atlantic and Pacific Oceans (Abadie
500 et al., 2017; Fitzsimmons et al., 2016). The Fe isotopic signature of AAIW is significantly modified at
501 the equator ($+0.22\text{‰}$, Radic et al., 2011) and close to Papua New Guinea ($+0.06$ to $+0.44\text{‰}$)
502 (Labatut et al., 2014; Radic et al., 2011). Abadie et al. (2017) observed that the light $\delta^{56}\text{Fe}$ values may
503 originate from the dilution of Upper Circumpolar Deep Water (UCDW; $\sim -0.8\text{‰}$), as AAIW originates
504 from the subduction of Antarctic Surface Water (AASW), which in turn results from the upwelling of
505 UCDW. We suggest that the $\delta^{56}\text{Fe}$ values we observed in AAIW are significantly modified by
506 remineralisation, sorption/desorption processes and sedimentary supply of new dFe.

507 At Station 2 NADW was present at depths between 1100 m and the seafloor (2656 m), with a $\delta^{56}\text{Fe}$
508 value of $+0.09$ to $+0.12\text{‰}$ ($n = 2$) and dFe concentrations of 1.3 to 1.7 nmol L^{-1} . Reported $\delta^{56}\text{Fe}$ values
509 for NADW differ significantly in the literature. In the North Atlantic Ocean, Conway and John (2014)
510 reported $\delta^{56}\text{Fe}$ values of $\sim +0.21\text{‰}$ at ~ 2000 m depth for a profile over the continental slope at $\sim 18^\circ$
511 W, and $\delta^{56}\text{Fe}$ values of $\sim +0.7\text{‰}$ at 2000 m depth at 30° W in the open ocean. Near Bermuda, the
512 $\delta^{56}\text{Fe}$ of NADW ranged from $+0.4$ to $+0.7\text{‰}$ (John and Adkins, 2012). NADW measured at ~ 3000 m
513 depth in the Southern Ocean has reported $\delta^{56}\text{Fe}$ values between $+0.2$ to $+0.3\text{‰}$ (Abadie et al., 2017).
514 This suggests that the isotopic composition of NADW is modified during its southwards journey. Such
515 processes might include: (i) exchange between the dissolved and particulate Fe pools (Ellwood et al.,
516 2015; John and Adkins, 2012; Labatut et al., 2014; Radic et al., 2011), and (ii) non-reductive
517 dissolution of sinking particles (Abadie et al., 2017).

518 Due to the short residence times and reactivity of Fe, and the supply of new Fe close to source
519 regions, the isotopic composition of the dissolved Fe pool is continuously modified and cannot be
520 applied as a conservative water mass tracer.

521 **4.5 The source of elevated dFe concentrations in low oxygen waters off the shelf**

522 The elevated dFe concentrations observed in the OMZ (between 40 and 900 m depth) at Station 2
523 may originate from offshore advection of high dFe containing shelf waters (Conway and John, 2014),
524 remineralisation of sinking particles (Fitzsimmons et al., 2013), and the net release of dFe from
525 particle surfaces (Milne et al., 2017). $\delta^{56}\text{Fe}$ values exhibited a negative correlation with dFe

526 concentrations, suggesting that most of the isotopic variations observed at our study site can
527 explained with mixing between high dFe concentration, low $\delta^{56}\text{Fe}$ shelf waters and low dFe
528 concentration, high $\delta^{56}\text{Fe}$ offshore water masses (Figure 6a). On the shelf, a positive correlation
529 between oxygen concentrations and $\delta^{56}\text{Fe}$ values could be an artefact due to larger amounts of
530 oxygen being consumed in deeper waters combined with poor ventilation indicates that redox
531 processes might have been dominating the dFe isotopic signatures (Figure 6b). However, this good
532 correlation disappeared on the slope, which suggests that elevated dFe concentrations were not
533 solely linked to low oxygen concentrations in waters off the shelf. We cannot assume that isotopic
534 signatures are solely governed by mixing processes, and hence, explore other possibilities below.

535 We have estimated the amount of dFe released to the water column due to remineralisation
536 processes, and this was up to 2.1 nmol L^{-1} within low oxygen waters on the slope (Figure 5; section
537 4.3). The contribution of remineralisation to the dFe concentrations measured in low oxygen waters
538 was 25 to 40 % (average 33 ± 5 , $n = 10$) on the shelf, 56 to 170 % (average 88 ± 36 %, $n = 11$) at
539 Station 3 and 94 to 150 % (average 118 ± 22 , $n = 9$) at Station 2. Hence, the importance of
540 remineralised dFe increased with distance from the shelf. The AOU was positively correlated with
541 dFe concentrations in all profiles, where shelf and slope stations lie on different slopes, which could
542 be a result of different phytoplankton community structures that have different Fe requirements
543 between these regions (Figure 7a). Highest remineralisation dFe contributions were correlated to
544 highest $\delta^{56}\text{Fe}$ values on the slope (Figure 7b). Hence, the high $\delta^{56}\text{Fe}$ values (-0.06 to 0.41 ‰, average
545 $+0.1 \pm 0.3$ ‰, $n = 7$) observed in oxygen low waters at Station 2 were mainly provided through
546 remineralisation of sinking organic matter.

547 “Excess” dFe (dFe supplied from processes other than remineralisation) is highest on the shelf
548 (Figure 5) and correlates with low $\delta^{56}\text{Fe}$ values on the slope (Figure 7b). Due to the overall
549 association to low $\delta^{56}\text{Fe}$ values, excess dFe can be mainly attributed to benthic inputs from
550 sediments. However, it is evident that excess dFe was composed of additional sources, as well as
551 benthic sources, on the shelf because excess dFe correlates with higher (instead of lower) $\delta^{56}\text{Fe}$
552 values (Figure 7b). The higher $\delta^{56}\text{Fe}$ values on the shelf were most likely due to the presence of
553 aerosol inputs and increased NRD of lithogenic material towards the surface ocean (as discussed in
554 section 4.2). On the shelf, the excess dFe was $2.4 \pm 0.8 \text{ nmol L}^{-1}$ ($n = 10$) with a maxima at 4.7 nmol L^{-1} ,
555 which represented as much as 75 % of dFe supplied to the water column by processes other than
556 remineralisation. This is also where lowest $\delta^{56}\text{Fe}$ values (-0.33 to -0.20 ‰) were observed below 40 m
557 depth (Figure 4), indicative of a strong benthic dFe source. On the slope, an average of $0.6 \pm 0.7 \text{ nmol L}^{-1}$
558 dFe ($n = 11$) and up to 1.6 nmol L^{-1} at 500 and 800 m depth could have been supplied by benthic
559 inputs to low oxygen waters at Station 3. Where excess dFe was highest at Station 3, $\delta^{56}\text{Fe}$ values

560 were also lowest (as low as -0.32 ‰ at 500 m depth), indicating a benthic source. At Station 2, there
561 was generally no excess dFe within low oxygen waters, so relatively high dFe concentrations are
562 associated with remineralisation. A small excess dFe concentration (0.12 nmol L⁻¹) at 200 m depth
563 was associated with a lower $\delta^{56}\text{Fe}$ value (-0.06 ‰), which can be attributed to a dilute benthic
564 influence at Station 2.

565 Scavenging of dFe onto biogenic and non-biogenic particles and exchange of Fe between the
566 dissolved and particulate phases are continuous processes within the water column and are likely to
567 overprint the isotopic signatures of benthic/atmospheric inputs and remineralisation. However, we
568 are not able to assess the effects of these processes in this study and assume that the associated
569 isotopic fractionation was small (Ellwood et al., 2015; Labatut et al., 2014; Radic et al., 2011).

570 Benthic dFe inputs from shelf and slope sediments and, to a lower extent at the time of our study,
571 atmospheric dFe inputs therefore appear to make an important contribution to the supply of “new”
572 dFe to the study area. We observe that waters containing high dFe concentrations and light isotopic
573 compositions are transported off the shelf to the slope region, which could be facilitated by the
574 westward flowing NECC and the nNECC. This assumption is confirmed by relatively high horizontal
575 dFe fluxes below the SML on the shelf (5185 $\mu\text{mol dFe m}^{-2} \text{d}^{-1}$) and slope (94.4 $\mu\text{mol dFe m}^{-2} \text{d}^{-1}$ at
576 Station 3) regions (Figure 8; Milne et al., 2017). The benthic isotopic signal of dFe is considerably
577 weakened at Station 2, as is the horizontal flux (21.5 $\mu\text{mol dFe m}^{-2} \text{d}^{-1}$ at Station 2 ;Milne et al., 2017),
578 ~37 km from the shelf stations. Likewise, remineralisation processes gain importance in the supply of
579 dFe to the OMZ with distance from the shelf. We suggest that a considerable proportion of the
580 recycled dFe is initially sourced from benthic and (to a minor degree at the time of sampling)
581 atmospheric inputs in our study area. Here we observed a snapshot of what could be the repetition
582 of continuous cycles of upwelling of high dFe bottom waters, followed by biological uptake, particle
583 sinking and remineralisation (followed by upwelling, etc), which leads to a net shift towards heavier
584 dFe isotopic compositions of the initially isotopically light benthic signal within the OMZ as moving
585 offshore (Figure 8). We envision that a significant part of sinking organic material is not remineralised
586 within the OMZ and is exported towards deeper waters, because remineralisation rates may be low
587 in OMZs (Cavan et al., 2017). Hence, the supply of new Fe (benthic and atmospheric) must play an
588 important role in maintaining the high Fe concentrations in the tropical North Atlantic OMZ.

589 Our results confirm previous studies of dFe concentrations, that inferred that remineralisation plays
590 a key role in the supply of dFe to the subsurface waters of offshore regions of the tropical Atlantic
591 OMZ (Fitzsimmons et al., 2013; Rijkenberg et al., 2012). These studies observed a near constant slope
592 between dFe and AOU, that indicated that the main dFe source was from remineralisation from

593 sinking material with a fixed Fe:C ratio. Rijkenberg et al. (2012) observed a shift to higher Fe:C ratios
594 north of 25 °N, indicative of external sources, which were attributed to shelf inputs.

595 Our results are partly consistent with a study north of Cape Verde islands that suggest that a shelf
596 signal may be observed up to 1000 km outside the OMZ in the open ocean (with $O_2 > 160 \mu\text{mol kg}^{-1}$)
597 (Conway and John, 2014). They suggest that 20 to 30 % of the dFe found in the water column on the
598 continental margins originates from reductive sediments. However, Conway and John (2014)
599 selected the $\delta^{56}\text{Fe}$ value of -2.4 ‰ from the Californian margin (John et al., 2012) as the benthic dFe
600 endmember to calculate its contribution to the entire ocean section. Our study indicates that the
601 $\delta^{56}\text{Fe}$ value of benthic supplied dFe must be closer to -0.3 ‰ on the eastern tropical Atlantic margin.
602 However, here we demonstrate that remineralisation processes can overprint dFe advected from the
603 shelf considerably, hence mass balance calculations using Fe isotopes should be applied with caution.

604 5. Conclusions

605 Our study confirms that remineralisation plays an important role in recycling Fe within the tropical
606 North Atlantic OMZ, but, in contrast to previous work, we provide evidence of significant benthic dFe
607 inputs to low oxygen waters. At times of low atmospheric dust depositions, we suggest that “new” Fe
608 is initially supplied by benthic inputs, and that consecutive cycles of bottom water upwelling,
609 biological uptake, and remineralisation of sinking of organic matter lead to the enhanced dFe
610 concentrations observed in the eastern boundary tropical North Atlantic OMZ. We also suggest that
611 benthic supplied dFe must be stabilised by complexation to organic ligands.

612 It is certain that regeneration of sinking organic material from the highly productive surface ocean is
613 key in maintaining high dFe concentrations within the tropical Atlantic OMZ, and that upwelling can
614 act as a transport vector to the surface ocean. Atmospheric dust deposition was low during the time
615 of our study but is known to be highly variable. The relative importance of new Fe provided from
616 atmospheric versus benthic Fe inputs to the surface ocean of the tropical North Atlantic as an annual
617 mean remains uncertain.

618 Because oxygen concentrations in seawater may have an influence on remineralisation rates and Fe
619 speciation, the decline in oxygen concentrations due to global warming may have significant
620 consequences on Fe cycling. This needs to be investigated and incorporated into future modelling
621 efforts of the linkages between biogeochemical cycles and climate.

622 6. Acknowledgements

623 We gratefully acknowledge the support of the captain and crew of *RRS Discovery* throughout cruise
624 D361. We also thank NMF staff for their technical assistance on-board. We thank the rest of the trace
625 metal sampling team Maeve C Lohan, Angela Milne and Felix Morales for their hard work on-board.
626 We thank Eithne Tynan for pH data and Alexander Forryan for help with CTD data.

627 7. Funding

628 This study was funded by the UK National Environmental Research Council (NE/G015732/1) and the
629 Atlantic Meridional Transect consortium (243). JKK's PhD studentship was funded by the Graduate
630 School of the National Oceanography Centre and NERC National Capability Funds.

631 8. List of tables

632 Table 1: $\delta^{56}\text{Fe}$ data and supporting parameters. dFe data are from (Milne et al., 2017).

633 Table 2: Estimates for dust supplied dFe concentrations ($d\text{Fe}_{\text{dust}}$) in the surface mixed layer (SML) and
634 dust derived dFe fluxes (in $\mu\text{mol Fe m}^{-2} \text{d}^{-1}$) from dAl measurements. Measured dFe ($d\text{Fe}_{\text{meas}}$) values
635 are from Schlosser et al. (2014). The SML depth (SMLD) was calculated using the approach in
636 Monterey and Levitus (1997). The SMLD for samples F-46, F-47 and F-49 were not measured and
637 estimated to be 11 m.

638 9. List of figures

639 Figure 1: Maps showing positions of sampling stations on the shelf and slope off the coast of Senegal
640 in the tropical North Atlantic Ocean. The main upper ocean circulation was adapted from (Stramma
641 et al., 2008a) and is shown by the grey lines. The red dotted line shows the $70 \mu\text{mol kg}^{-1}$ dissolved
642 oxygen contour of the OMZ at 400 m depth (Stramma et al., 2008b). NECC = North Equatorial
643 Countercurrent; nNECC = norther NECC; NEUC = North Equatorial Undercurrent; GD = Guinea Dome.

644 Figure 2: Hydrographic properties (potential temperature, practical salinity, density and dissolved
645 oxygen) at stations 2, 3, 4 and 5. Water masses are delimited with green lines. TSW = Tropical Surface
646 Water; SACW = South Atlantic Central Water; AAIW = Antarctic Intermediate Water; NADW = North
647 Atlantic Deep Water.

648 Figure 3: Phosphate vs dFe concentrations for all stations. Note that the slope of the correlation is
649 different in shelf waters (stations 4 and 5) and slope waters (stations 2 and 3).

650 Figure 4: Profiles of Chl-a, transmittance, oxygen concentrations, dFe concentrations and $\delta^{56}\text{Fe}$ values
651 at a) slope stations 2 and 3 and b) shelf stations 4 and 5. dFe data are from (Milne et al., 2017). Note
652 change of scale for dFe concentrations between upper and lower plots. The average $\delta^{56}\text{Fe}$ value of
653 the continental crust is shown as a vertical black line ($+0.09 \pm 0.10 \text{ ‰}$, 2 SD, $n = 46$; Beard et al.,
654 2003).

655 Figure 5: Proportions of calculated remineralised dFe concentrations, relative to measured dFe
656 concentrations (a) on the shelf and (b) on the slope.

657 Figure 6: Relationship of (a) $\delta^{56}\text{Fe}$ vs dFe; and (b) $\delta^{56}\text{Fe}$ vs O_2 on the shelf (stations 4 and 5) and on the
658 slope (stations 2 and 3). The average $\delta^{56}\text{Fe}$ value of the continental crust ($+0.09 \pm 0.10 \text{ ‰}$; Beard et
659 al., 2003) is shown with black lines. Linear regressions of the $\delta^{56}\text{Fe}$ vs dFe relationship for the entire
660 data set and of the $\delta^{56}\text{Fe}$ vs O_2 on the shelf are shown with dotted lines and their equations are
661 displayed.

662 Figure 7: (a) Relationship between dFe and AOU in the upper 1000 m of the water column and (b)
663 relationship between $\delta^{56}\text{Fe}$ and remineralised dFe ($\text{dFe}_{\text{remin}}$) for the shelf (stations 4 and 5) and the
664 slope (stations 2 and 3) regions. The average $\delta^{56}\text{Fe}$ value of the continental crust ($+0.09 \pm 0.10 \text{ ‰}$;
665 Beard et al., 2003) is shown with a black line in (b). Linear regressions are shown with dotted lines
666 and their equations are displayed.

667 Figure 8: Simplified view of the Fe cycle in our study area. Shelf sediments supply dFe with a light
668 isotopic composition ($\downarrow \delta^{56}\text{Fe}$) to bottom waters. dFe is supplied to the surface mixed layer (SML) by
669 atmospheric dust deposition and upwelled bottom waters, where phytoplankton takes up dFe with a
670 relatively heavy isotopic composition ($\uparrow \delta^{56}\text{Fe}$). Remineralisation of sinking organic material leads to
671 the release of dFe with a relatively heavy isotopic composition, which is mixed with benthic dFe
672 inputs and upwelled to the SML, where it is mixed with atmospheric dFe inputs. The flux of benthic
673 dFe decreases with distance from the coast. The continuous recycling of dFe by biological uptake and
674 remineralisation leads to increasingly heavy isotopic compositions of dFe in the water column
675 moving offshore. Atmospheric dust inputs (fluxes in $\mu\text{mol dFe m}^{-2} \text{ d}^{-1}$, in brown) to the SML,
676 calculated from dAl concentrations, were low at the time of sampling but are potentially higher at
677 other times of the year (Croot et al., 2004). Fluxes of vertical transport to the SML (white) and
678 horizontal transport between the bottom of the SML and 500 m depth (yellow) are from Milne et al.
679 (2017) and are in $\mu\text{mol dFe m}^{-2} \text{ d}^{-1}$.

680 10. References

- 681 Abadie, C., Lacan, F., Radic, A., Pradoux, C. and Poitrasson, F. (2017) Iron isotopes reveal
682 distinct dissolved iron sources and pathways in the intermediate versus deep Southern Ocean.
683 *Proceedings of the National Academy of Sciences* 114, 858-863.
- 684 Beard, B.L., Johnson, C.M., Von Damm, K.L. and Poulson, R.L. (2003) Iron isotope constraints on
685 Fe cycling and mass balance in oxygenated Earth oceans. *Geology* 31, 629-632.
- 686 Bergquist, B.A. and Boyle, E.A. (2006) Iron isotopes in the Amazon River system: Weathering
687 and transport signatures. *Earth. Planet. Sci. Lett.* 248, 54-68.
- 688 Berman-Frank, I., Cullen, J.T., Shaked, Y., Sherrell, R.M. and Falkowski, P.G. (2001) Iron
689 availability, cellular iron quotas, and nitrogen fixation in *Trichodesmium*. *Limnol. Oceanogr.* 46, 1249-
690 1260.
- 691 Boyd, P.W. and Ellwood, M.J. (2010) The biogeochemical cycle of iron in the ocean. *Nat.*
692 *Geosci.* 3.
- 693 Boyle, E.A., John, S., Abouchami, W., Adkins, J.F., Echevoyen-Sanz, Y., Ellwood, M., Flegal, A.R.,
694 Fornace, K., Gallon, C., Galer, S., Gault-Ringold, M., Lacan, F., Radic, A., Rehkemper, M., Rouxel, O.,
695 Sohrin, Y., Stirling, C., Thompson, C., Vance, D., Xue, Z. and Zhao, Y. (2012) GEOTRACES IC1 (BATS)
696 contamination-prone trace element isotopes Cd, Fe, Pb, Zn, Cu, and Mo intercalibration. *Limnol.*
697 *Oceanogr. Meth.* 10, 653-665.
- 698 Brandt, P., Hormann, V., Kortzinger, A., Visbeck, M., Krahnemann, G., Stramma, L., Lumpkin, R.
699 and Schmid, C. (2010) Changes in the Ventilation of the Oxygen Minimum Zone of the Tropical North
700 Atlantic. *J. Phys. Oceanogr.* 40, 1784-1801.
- 701 Brown, M.T. and Bruland, K.W. (2008) An improved flow-injection analysis method for the
702 determination of dissolved aluminum in seawater. *Limnol. Oceanogr. Meth.* 6, 87-95.
- 703 Buck, C.S., Landing, W.M., Resing, J.A. and Measures, C.I. (2010) The solubility and deposition
704 of aerosol Fe and other trace elements in the North Atlantic Ocean: Observations from the A16N
705 CLIVAR/CO(2) repeat hydrography section. *Mar. Chem.* 120, 57-70.
- 706 Cavan, E.L., Trimmer, M., Shelley, F. and Sanders, R. (2017) Remineralization of particulate
707 organic carbon in an ocean oxygen minimum zone. 8, 14847.
- 708 Chan, F., Barth, J.A., Lubchenco, J., Kirincich, A., Weeks, H., Peterson, W.T. and Menge, B.A.
709 (2008) Emergence of anoxia in the California current large marine ecosystem. *Science* 319, 920-920.

710 Chever, F., Rouxel, O.J., Croot, P.L., Ponzevera, E., Wuttig, K. and Auro, M. (2015) Total
711 dissolvable and dissolved iron isotopes in the water column of the Peru upwelling regime. *Geochim.*
712 *Cosmochim. Acta* 162, 66-82.

713 Coale, K.H., Johnson, K.S., Chavez, F.P., Buesseler, K.O., Barber, R.T., Brzezinski, M.A., Cochlan,
714 W.P., Millero, F.J., Falkowski, P.G., Bauer, J.E., Wanninkhof, R.H., Kudela, R.M., Altabet, M.A., Hales,
715 B.E., Takahashi, T., Landry, M.R., Bidigare, R.R., Wang, X.J., Chase, Z., Strutton, P.G., Friederich, G.E.,
716 Gorbunov, M.Y., Lance, V.P., Hilting, A.K., Hiscock, M.R., Demarest, M., Hiscock, W.T., Sullivan, K.F.,
717 Tanner, S.J., Gordon, R.M., Hunter, C.N., Elrod, V.A., Fitzwater, S.E., Jones, J.L., Tozzi, S., Koblizek, M.,
718 Roberts, A.E., Herndon, J., Brewster, J., Ladizinsky, N., Smith, G., Cooper, D., Timothy, D., Brown, S.L.,
719 Selph, K.E., Sheridan, C.C., Twining, B.S. and Johnson, Z.I. (2004) Southern ocean iron enrichment
720 experiment: Carbon cycling in high- and low-Si waters. *Science* 304, 408-414.

721 Conway, T.M. and John, S.G. (2014) Quantification of dissolved iron sources to the North
722 Atlantic Ocean. *Nature advance online publication*.

723 Croot, P.L., Streu, P. and Baker, A.R. (2004) Short residence time for iron in surface seawater
724 impacted by atmospheric dry deposition from Saharan dust events. *Geophysical Research Letters* 31,
725 L23S08.

726 Damshäuser, A., Wagener, T. and Croot, P.L. (2011) Surface water dissolved aluminum and
727 titanium: Tracers for specific time scales of dust deposition to the Atlantic? *Geophysical Research*
728 *Letters* 38.

729 Dideriksen, K., Baker, J.A. and Stipp, S.L.S. (2008) Equilibrium Fe isotope fractionation between
730 inorganic aqueous Fe(III) and the siderophore complex, Fe(III)-desferrioxamine B. *Earth. Planet. Sci.*
731 *Lett.* 269, 280-290.

732 Ellwood, M.J., Hutchins, D.A., Lohan, M.C., Milne, A., Nasemann, P., Nodder, S.D., Sander, S.G.,
733 Strzepek, R., Wilhelm, S.W. and Boyd, P.W. (2015) Iron stable isotopes track pelagic iron cycling
734 during a subtropical phytoplankton bloom. *Proceedings of the National Academy of Sciences* 112,
735 E15-E20.

736 Escube, R., Rouxel, O.J., Sholkovitz, E. and Donard, O.F.X. (2009) Iron isotope systematics in
737 estuaries: The case of North River, Massachusetts (USA). *Geochim. Cosmochim. Acta* 73, 4045-4059.

738 Falkowski, P.G. (1997) Evolution of the nitrogen cycle and its influence on the biological
739 sequestration of CO₂ in the ocean. *Nature* 387, 272-275.

740 Fitzsimmons, J.N., Conway, T.M., Lee, J.M., Kayser, R., Thyng, K.M., John, S.G. and Boyle, E.A.
741 (2016) Dissolved iron and iron isotopes in the southeastern Pacific Ocean. *Global Biogeochem. Cycles*
742 30, 1372-1395.

743 Fitzsimmons, J.N., Zhang, R. and Boyle, E.A. (2013) Dissolved iron in the tropical North Atlantic
744 Ocean. *Mar. Chem.* 154, 87-99.

745 Gehlen, M., Beck, L., Calas, G., Flank, A.M., Van Bennekom, A.J. and Van Beusekom, J.E.E.
746 (2002) Unraveling the atomic structure of biogenic silica: Evidence of the structural association of Al
747 and Si in diatom frustules. *Geochim. Cosmochim. Acta* 66, 1601-1609.

748 Gledhill, M. and Buck, K.N. (2012) The organic complexation of iron in the marine
749 environment: a review. *Frontiers in Microbiology* 3.

750 Goldberg, E.D. (1954) Marine Geochemistry 1. Chemical Scavengers of the Sea. *The Journal of*
751 *Geology* 62, 249-265.

752 Henkel, S., Kasten, S., Poulton, S.W. and Staubwasser, M. (2016) Determination of the stable
753 iron isotopic composition of sequentially leached iron phases in marine sediments. *Chem. Geol.* 421,
754 93-102.

755 Hioki, N., Kuma, K., Morita, Y., Sasayama, R., Ooki, A., Kondo, Y., Obata, H., Nishioka, J.,
756 Yamashita, Y., Nishino, S., Kikuchi, T. and Aoyama, M. (2014) Laterally spreading iron, humic-like
757 dissolved organic matter and nutrients in cold, dense subsurface water of the Arctic Ocean. 4, 6775.

758 Homoky, W.B., John, S.G., Conway, T.M. and Mills, R.A. (2013) Distinct iron isotopic signatures
759 and supply from marine sediment dissolution. *Nat Commun* 4.

760 Homoky, W.B., Severmann, S., McManus, J., Berelson, W.M., Riedel, T.E., Statham, P.J. and
761 Mills, R.A. (2012) Dissolved oxygen and suspended particles regulate the benthic flux of iron from
762 continental margins. *Mar. Chem.* 134, 59-70.

763 Homoky, W.B., Severmann, S., Mills, R.A., Statham, P.J. and Fones, G.R. (2009) Pore-fluid Fe
764 isotopes reflect the extent of benthic Fe redox recycling: Evidence from continental shelf and deep-
765 sea sediments. *Geology* 37, 751-754.

766 Jickells, T.D., An, Z.S., Andersen, K.K., Baker, A.R., Bergametti, G., Brooks, N., Cao, J.J., Boyd,
767 P.W., Duce, R.A., Hunter, K.A., Kawahata, H., Kubilay, N., laRoche, J., Liss, P.S., Mahowald, N.,
768 Prospero, J.M., Ridgwell, A.J., Tegen, I. and Torres, R. (2005) Global iron connections between desert
769 dust, ocean biogeochemistry, and climate. *Science* 308, 67-71.

770 John, S.G. and Adkins, J. (2012) The vertical distribution of iron stable isotopes in the North
771 Atlantic near Bermuda. *Global Biogeochem. Cycles* 26.

772 John, S.G. and Adkins, J.F. (2010) Analysis of dissolved iron isotopes in seawater. *Mar. Chem.*
773 119, 65-79.

774 John, S.G., Helgoe, J., Townsend, E., Weber, T., DeVries, T., Tagliabue, A., Moore, K., Lam, P.,
775 Marsay, C.M. and Till, C. (2017) Biogeochemical cycling of Fe and Fe stable isotopes in the Eastern
776 Tropical South Pacific. *Mar. Chem.*

777 John, S.G., Mendez, J., Moffett, J. and Adkins, J. (2012) The flux of iron and iron isotopes from
778 San Pedro Basin sediments. *Geochim. Cosmochim. Acta* 93, 14-29.

779 Jones, M.E., Beckler, J.S. and Taillefert, M. (2011) The flux of soluble organic-iron(III) complexes
780 from sediments represents a source of stable iron(III) to estuarine waters and to the continental
781 shelf. *Limnol. Oceanogr.* 56, 1811-1823.

782 Karstensen, J., Stramma, L. and Visbeck, M. (2008) Oxygen minimum zones in the eastern
783 tropical Atlantic and Pacific oceans. *Prog. Oceanogr.* 77, 331-350.

784 Keeling, R.F., Koertzing, A. and Gruber, N. (2010) Ocean Deoxygenation in a Warming World.
785 *Annual Review of Marine Science* 2, 199-229.

786 Klar, J.K., Homoky, W.B., Statham, P.J., Birchill, A.J., Harris, E.L., Woodward, E.M.S., Silburn, B.,
787 Cooper, M.J., James, R.H., Connelly, D.P., Chever, F., Lichtschlag, A. and Graves, C. (2017a) Stability of
788 dissolved and soluble Fe(II) in shelf sediment pore waters and release to an oxic water column.
789 *Biogeochemistry*.

790 Klar, J.K., James, R.H., Gibbs, D., Lough, A., Parkinson, I., Milton, J.A., Hawkes, J.A. and Connelly,
791 D.P. (2017b) Isotopic signature of dissolved iron delivered to the Southern Ocean from hydrothermal
792 vents in the East Scotia Sea. *Geology* 45, 351-354.

793 Klunder, M.B., Laan, P., Middag, R., de Baar, H.J.W. and Bakker, K. (2012) Dissolved iron in the
794 Arctic Ocean: Important role of hydrothermal sources, shelf input and scavenging removal. *J.*
795 *Geophys. Res.-Oceans* 117.

796 Klunder, M.B., Laan, P., Middag, R., De Baar, H.J.W. and van Ooijen, J.C. (2011) Dissolved iron
797 in the Southern Ocean (Atlantic sector). *Deep Sea Research Part II: Topical Studies in Oceanography*
798 58, 2678-2694.

799 Kramer, J., Laan, P., Sarthou, G., Timmermans, K.R. and de Baar, H.J.W. (2004) Distribution of
800 dissolved aluminium in the high atmospheric input region of the subtropical waters of the North
801 Atlantic Ocean. *Mar. Chem.* 88, 85-101.

802 Labatut, M., Lacan, F., Pradoux, C., Chmeleff, J., Radic, A., Murray, J.W., Poitrasson, F.,
803 Johansen, A.M. and Thil, F. (2014) Iron sources and dissolved-particulate interactions in the seawater
804 of the Western Equatorial Pacific, iron isotope perspectives. *Global Biogeochem. Cycles* 28, 1044-
805 1065.

806 Lacan, F., Radic, A., Jeandel, C., Poitrasson, F., Sarthou, G., Pradoux, C. and Freydisier, R. (2008)
807 Measurement of the isotopic composition of dissolved iron in the open ocean. *Geophysical Research*
808 *Letters* 35.

809 Lacan, F., Radic, A., Labatut, M., Jeandel, C., Poitrasson, F., Sarthou, G., Pradoux, C., Chmeleff,
810 J. and Freydisier, R. (2010) High-Precision Determination of the Isotopic Composition of Dissolved Iron
811 in Iron Depleted Seawater by Double Spike Multicollector-ICPMS. *Anal. Chem.* 82, 7103-7111.

812 Le Quéré, C., Andres, R.J., Boden, T., Conway, T., Houghton, R.A., House, J.I., Marland, G.,
813 Peters, G.P., van der Werf, G.R., Ahlström, A., Andrew, R.M., Bopp, L., Canadell, J.G., Ciais, P., Doney,
814 S.C., Enright, C., Friedlingstein, P., Huntingford, C., Jain, A.K., Jourdain, C., Kato, E., Keeling, R.F., Klein
815 Goldewijk, K., Levis, S., Levy, P., Lomas, M., Poulter, B., Raupach, M.R., Schwinger, J., Sitch, S.,
816 Stocker, B.D., Viovy, N., Zaehle, S. and Zeng, N. (2013) The global carbon budget 1959–2011. *Earth*
817 *Syst. Sci. Data* 5, 165-185.

818 Liu, X. and Millero, F.J. (2002) The solubility of iron in seawater. *Mar. Chem.* 77, 43-54.

819 Lomnitz, U. (2017) Biogeochemical cycling of iron and phosphorus under low oxygen
820 conditions, Mathematisch-Naturwissenschaftliche Fakultät. Christian-Albrechts-Universität zu Kiel,
821 Kiel.

822 Mackey, D.J., O'Sullivan, J.E.O. and Watson, R.J. (2002) Iron in the western Pacific: a riverine or
823 hydrothermal source for iron in the Equatorial Undercurrent? *Deep Sea Research Part I:*
824 *Oceanographic Research Papers* 49, 877-893.

825 Marsay, C.M., Sedwick, P.N., Dinniman, M.S., Barrett, P.M., Mack, S.L. and McGillicuddy, D.J.
826 (2014) Estimating the benthic efflux of dissolved iron on the Ross Sea continental shelf. *Geophysical*
827 *Research Letters* 41, 7576-7583.

828 Martin, J.H. (1990) Glacial-interglacial CO₂ change: the iron hypothesis. *Paleoceanography* 5,
829 1-13.

830 Martin, J.H. and Fitzwater, S.E. (1988) Iron-deficiency limits phytoplankton growth in the
831 northeast Pacific Subarctic. *Nature* 331, 341-343.

832 Martin, J.H., Knauer, G.A., Karl, D.M. and Broenkow, W.W. (1987) VERTEX: carbon cycling in
833 the northeast Pacific. *Deep Sea Research Part A. Oceanographic Research Papers* 34, 267-285.

834 Mead, C., Herckes, P., Majestic, B.J. and Anbar, A.D. (2013) Source apportionment of aerosol
835 iron in the marine environment using iron isotope analysis. *Geophysical Research Letters* 40, 5722-
836 5727.

837 Measures, C.I. and Brown, E.T. (1996) Estimating dust input to the Atlantic Ocean using surface
838 water Al concentrations, in: Guerzoni, S., Chester, R. (Eds.), *The Impact of Desert Dust Across the*
839 *Mediterranean*. Kluwer Academic Publishers, Dordrecht, p. 389.

840 Millero, F.J., Sotolongo, S. and Izaguirre, M. (1987) The oxidation-kinetics of Fe(II) in seawater.
841 *Geochim. Cosmochim. Acta* 51, 793-801.

842 Milne, A., Schlosser, C., Wake, B.D., Achterberg, E.P., Chance, R., Baker, A.R., Forryan, A. and
843 Lohan, M.C. (2017) Particulate phases are key in controlling dissolved iron concentrations in the
844 (sub)tropical North Atlantic. *Geophysical Research Letters* 44, 2377-2387.

845 Monterey, G.I. and Levitus, S. (1997) Seasonal variability of mixed layer depth for the world
846 ocean. US Department of Commerce, National Oceanic and Atmospheric Administration, National
847 Environmental Satellite, Data, and Information Service.

848 Moore, J.K., Doney, S.C., Glover, D.M. and Fung, I.Y. (2001) Iron cycling and nutrient-limitation
849 patterns in surface waters of the World Ocean. *Deep Sea Research Part II: Topical Studies in*
850 *Oceanography* 49, 463-507.

851 Moran, S.B. and Moore, R.M. (1992) Kinetics of the removal of dissolved aluminum by diatoms
852 in seawater: A comparison with thorium. *Geochim. Cosmochim. Acta* 56, 3365-3374.

853 Morgan, J.L.L., Wasylenki, L.E., Nuester, J. and Anbar, A.D. (2010) Fe Isotope Fractionation
854 during Equilibration of Fe-Organic Complexes. *Environmental Science & Technology* 44, 6095-6101.

855 Nishioka, J. and Obata, H. (2017) Dissolved iron distribution in the western and central
856 subarctic Pacific: HNLC water formation and biogeochemical processes. *Limnol. Oceanogr.*, n/a-n/a.

857 Noffke, A., Hensen, C., Sommer, S., Scholz, F., Bohlen, L., Mosch, T., Graco, M. and Wallmann,
858 K. (2012) Benthic iron and phosphorus fluxes across the Peruvian oxygen minimum zone. *Limnol.*
859 *Oceanogr.* 57, 851-867.

860 Patey, M.D., Achterberg, E.P., Rijkenberg, M.J. and Pearce, R. (2015) Aerosol time-series
861 measurements over the tropical Northeast Atlantic Ocean: Dust sources, elemental composition and
862 mineralogy. *Mar. Chem.* 174, 103-119.

863 Planquette, H., Statham, P.J., Fones, G.R., Charette, M.A., Moore, C.M., Salter, I., Nedelec, F.H.,
864 Taylor, S.L., French, M., Baker, A.R., Mahowald, N. and Jickells, T.D. (2007) Dissolved iron in the
865 vicinity of the Crozet Islands, Southern Ocean. *Deep-Sea Res. Part II-Top. Stud. Oceanogr.* 54, 1999-
866 2019.

867 Poitrasson, F., Vieira, L.C., Seyler, P., Pinheiro, G.M.D., Mulholland, D.S., Bonnet, M.P.,
868 Martinez, J.M., Lima, B.A., Boaventura, G.R., Chmeleff, J., Dantas, E.L., Guyot, J.L., Mancini, L.,
869 Pimentel, M.M., Santos, R.V., Sondag, F. and Vauchel, P. (2014) Iron isotope composition of the bulk
870 waters and sediments from the Amazon River Basin. *Chem. Geol.* 377, 1-11.

871 Radic, A., Lacan, F. and Murray, J.W. (2011) Iron isotopes in the seawater of the equatorial
872 Pacific Ocean: New constraints for the oceanic iron cycle. *Earth. Planet. Sci. Lett.* 306, 1-10.

873 Resing, J.A. and Measures, C.I. (1994) Fluorometric determination of Al in seawater by Flow-
874 Injection-Analysis with in-line preconcentration. *Anal. Chem.* 66, 4105-4111.

875 Resing, J.A., Sedwick, P.N., German, C.R., Jenkins, W.J., Moffett, J.W., Sohst, B.M. and
876 Tagliabue, A. (2015) Basin-scale transport of hydrothermal dissolved metals across the South Pacific
877 Ocean. *Nature* 523, 200-203.

878 Rijkenberg, M.J.A., Middag, R., Laan, P., Gerringa, L.J.A., van Aken, H.M., Schoemann, V., de
879 Jong, J.T.M. and de Baar, H.J.W. (2014) The distribution of dissolved iron in the west atlantic ocean.
880 *PloS one* 9, e101323-e101323.

881 Rijkenberg, M.J.A., Steigenberger, S., Powell, C.F., van Haren, H., Patey, M.D., Baker, A.R. and
882 Achterberg, E.P. (2012) Fluxes and distribution of dissolved iron in the eastern (sub-) tropical North
883 Atlantic Ocean. *Global Biogeochem. Cycles* 26.

884 Rouxel, O., Shanks, W.C., Bach, W. and Edwards, K.J. (2008) Integrated Fe- and S-isotope study
885 of seafloor hydrothermal vents at East Pacific rise 9-10 degrees N. *Chem. Geol.* 252, 214-227.

886 Schlosser, C., Klar, J.K., Wake, B.D., Snow, J.T., Honey, D.J., Woodward, E.M.S., Lohan, M.C.,
887 Achterberg, E.P. and Moore, C.M. (2014) Seasonal ITCZ migration dynamically controls the location of
888 the (sub)tropical Atlantic biogeochemical divide. *Proceedings of the National Academy of Sciences*
889 111, 1438-1442.

890 Schmidtko, S., Stramma, L. and Visbeck, M. (2017) Decline in global oceanic oxygen content
891 during the past five decades. *Nature* 542, 335-339.

892 Schott, F.A., McCreary, J.P. and Johnson, G.C. (2004) Shallow Overturning Circulations of the
893 Tropical-Subtropical Oceans, Earth's Climate. American Geophysical Union, pp. 261-304.

894 Severmann, S., Johnson, C.M., Beard, B.L. and McManus, J. (2006) The effect of early
895 diagenesis on the Fe isotope compositions of porewaters and authigenic minerals in continental
896 margin sediments. *Geochim. Cosmochim. Acta* 70, 2006-2022.

897 Severmann, S., McManus, J., Berelson, W.M. and Hammond, D.E. (2010) The continental shelf
898 benthic iron flux and its isotope composition. *Geochim. Cosmochim. Acta* 74, 3984-4004.

899 Siedlecki, S.A., Mahadevan, A. and Archer, D.E. (2012) Mechanism for export of sediment-
900 derived iron in an upwelling regime. *Geophysical Research Letters* 39.

901 Siedler, G., Kuhl, A. and Zenk, W. (1987) The Madeira mode water. *J. Phys. Oceanogr.* 17, 1561-
902 1570.

903 Stramma, L., Brandt, P., Schafstall, J., Schott, F., Fischer, J. and Koertzing, A. (2008a) Oxygen
904 minimum zone in the North Atlantic south and east of the Cape Verde Islands. *J. Geophys. Res.-*
905 *Oceans* 113.

906 Stramma, L. and England, M. (1999) On the water masses and mean circulation of the South
907 Atlantic Ocean. *Journal of Geophysical Research: Oceans* 104, 20863-20883.

908 Stramma, L., Huttel, S. and Schafstall, J. (2005) Water masses and currents in the upper tropical
909 northeast Atlantic off northwest Africa. *J. Geophys. Res.-Oceans* 110.

910 Stramma, L., Johnson, G.C., Sprintall, J. and Mohrholz, V. (2008b) Expanding oxygen-minimum
911 zones in the tropical oceans. *Science* 320, 655-658.

912 Stramma, L. and Schott, F. (1999) The mean flow field of the tropical Atlantic Ocean. *Deep-Sea*
913 *Res. Part II-Top. Stud. Oceanogr.* 46, 279-303.

914 Tagliabue, A., Bowie, A.R., Boyd, P.W., Buck, K.N., Johnson, K.S. and Saito, M.A. (2017) The
915 integral role of iron in ocean biogeochemistry. *Nature* 543, 51-59.

916 Taylor, S.R. (1964) Abundance of chemical elements in the continental crust: a new table.
917 *Geochim. Cosmochim. Acta* 28, 1273-1285.

918 Twining, B.S., Rauschenberg, S., Morton, P.L. and Vogt, S. (2015) Metal contents of
919 phytoplankton and labile particulate material in the North Atlantic Ocean. *Prog. Oceanogr.* 137, Part
920 A, 261-283.

921 Ussher, S.J., Achterberg, E.P., Powell, C., Baker, A.R., Jickells, T.D., Torres, R. and Worsfold, P.J.
922 (2013) Impact of atmospheric deposition on the contrasting iron biogeochemistry of the North and
923 South Atlantic Ocean. *Global Biogeochem. Cycles* 27, 1096-1107.

924 Ussher, S.J., Achterberg, E.P., Sarthou, G., Laan, P., de Baar, H.J.W. and Worsfold, P.J. (2010)
925 Distribution of size fractionated dissolved iron in the Canary Basin. *Marine Environmental Research*
926 70, 46-55.

927 Ussher, S.J., Achterberg, E.P. and Worsfold, P.J. (2004) Marine Biogeochemistry of Iron.
928 *Environmental Chemistry* 1, 67-80.

929 Waeles, M., Baker, A.R., Jickells, T. and Hoogewerff, J. (2007) Global dust teleconnections:
930 aerosol iron solubility and stable isotope composition. *Environmental Chemistry* 4, 233-237.

931 Woodward, E.M.S. and Rees, A.P. (2001) Nutrient distributions in an anticyclonic eddy in the
932 northeast Atlantic Ocean, with reference to nanomolar ammonium concentrations. *Deep-Sea Res.*
933 *Part II-Top. Stud. Oceanogr.* 48, 775-793.

934

935

Table 1

Sample ID	Depth (m)	σ_θ (kg m ⁻³)	Oxygen ($\mu\text{mol kg}^{-1}$)	Salinity	pot T (°C)	water mass	dFe (nmol L ⁻¹)	2SD (nmol L ⁻¹)	$\delta^{56}\text{Fe}$ (‰)	2SD (‰)	Phosphate ($\mu\text{mol L}^{-1}$)	Nitrate ($\mu\text{mol L}^{-1}$)
<i>Station 4, Cast 11, 12.6120 N, -17.5728 E, 51 m bottom depth</i>												
11_12	25	25.66	158.5	35.71	18.61	TSW	2.5	0.2	0.03	0.04	0.97	13.51
11_11	38	25.79	119.8	35.69	18.01	TSW	3.36	0.08	-0.20	0.04	1.08	15.76
11_10	40	25.83	111.6	35.68	17.84	TSW	3.49	0.16	-0.32	0.04	1.12	16.14
11_09	49	25.91	93.1	35.67	17.48	SACW	3.82	0.06	-0.25	0.04	1.13	6.68
<i>Station 5, Cast 12, 12.5882 N, -17.5724 E, 164 m bottom depth</i>												
12_23	26	25.72	138.4	35.69	18.34	TSW	3.01	0.10	-0.11	0.05	1.10	15.48
12_21	36	25.79	116.8	35.68	18.01	TSW	2.99	0.13	-0.23	0.05	1.21	17.26
12_19	51	25.88	96.9	35.67	17.63	SACW	3.5	0.2	-0.16	0.05	1.25	18.03
12_17	66	25.93	81.2	35.66	17.37	SACW	3.75	0.06	-0.25	0.04	1.25	18.08
12_15	80	25.96	78.5	35.66	17.23	SACW	3.68	0.09	-0.31	0.05	1.29	18.89
12_13	107	26.18	68.8	35.62	16.22	SACW	6.3	0.5	-0.33	0.05	1.43	21.51
<i>Station 3, Cast 8, 12.6100 N, -17.7157 E, 1041 m bottom depth</i>												
8_21	199	26.54	71.9	35.44	13.94	SACW	1.81	0.02	0.06	0.08	1.59	25.63
8_20	300	26.85	59.3	35.39	12.22	SACW	2.58	0.02	-0.15	0.08	1.73	28.62
8_19	400	27.03	44.6	35.27	10.76	SACW	2.86	0.08	-0.19	0.04	1.98	32.82
8_18	500	27.14	48.9	35.10	9.38	SACW/AAIW	3.77	0.19	-0.32	0.04	2.17	34.79
8_17	599	27.21	60.1	34.89	7.83	AAIW	2.14	0.09	-0.08	0.04	2.33	36.72
8_16	699	27.28	74.0	34.84	7.08	AAIW	2.66	0.05	-0.30	0.04	1.91	30.81
8_14	899	27.38	99.5	34.79	6.06	AAIW	2.69	0.06	-0.26	0.04	2.32	34.88
8_13	1002	27.50	130.8	34.84	5.38	AAIW	2.90	0.18	-0.27	0.04	2.16	31.77
<i>Station 2, Cast 6, 12.5942 N, -17.9199 E, 2656 m bottom depth</i>												
6_21	198	26.63	70.5	35.41	13.39	SACW	1.85	0.10	-0.06	0.08	1.62	26.69
6_20	299	26.86	58.1	35.38	12.07	SACW	1.89	0.05	0.02	0.08	1.81	30.37
6_19	399	27.03	43.8	35.27	10.75	SACW	1.51	0.08	0.21	0.04	1.98	33.18
6_18	499	27.14	49.7	35.14	9.52	SACW/AAIW	1.40	0.04	0.41	0.04	2.19	35.37
6_17	599	27.22	58.5	34.93	7.93	AAIW	1.96	0.06	0.10	0.08	2.32	36.89
6_16	750	27.32	85.0	34.78	6.46	AAIW	1.82	0.05	0.12	0.08	2.37	36.55
6_15	900	27.40	111.1	34.76	5.64	AAIW	1.74	0.05	0.12	0.05		
6_12	1699	27.77	216.9	34.96	3.82	NADW	1.66	0.03	0.09	0.08	2.32	34.61
6_10	2625	27.86	237.6	34.94	2.77	NADW	1.33	0.03	0.12	0.08	1.60	22.76
									0.09	0.04	1.56	21.18

Table 2

Sample ID	Lat (°N)	Long (°E)	Stn	SMLD (m)	dAl _{meas} (nmol L ⁻¹)	SD	dFe _{meas} (nmol L ⁻¹)	SD	dFe _{dust} (nmol L ⁻¹)	SD	dust flux (μmol dFe m ⁻² d ⁻¹)	SD
F-44	12.590	-17.653	4 & 5	11	0.9	0.4	0.48	0.03	0.29	0.12	0.17	0.14
F-45	12.587	-17.714	3	19	2.1	0.4	0.45	0.02	0.70	0.13	0.71	0.50
F-46	12.586	-17.773	0	11	1.0	0.4			0.34	0.14	0.20	0.16
F-47	12.586	-17.831	0	11	2.4	0.4	0.76	0.02	0.78	0.14	0.46	0.32
F-48	12.585	-17.890	2	11	1.1	0.4	0.73	0.09	0.38	0.12	0.22	0.17
F-49	12.585	-17.949	0	11	2.1	0.4	0.83	0.03	0.70	0.12	0.41	0.29

Figure 1

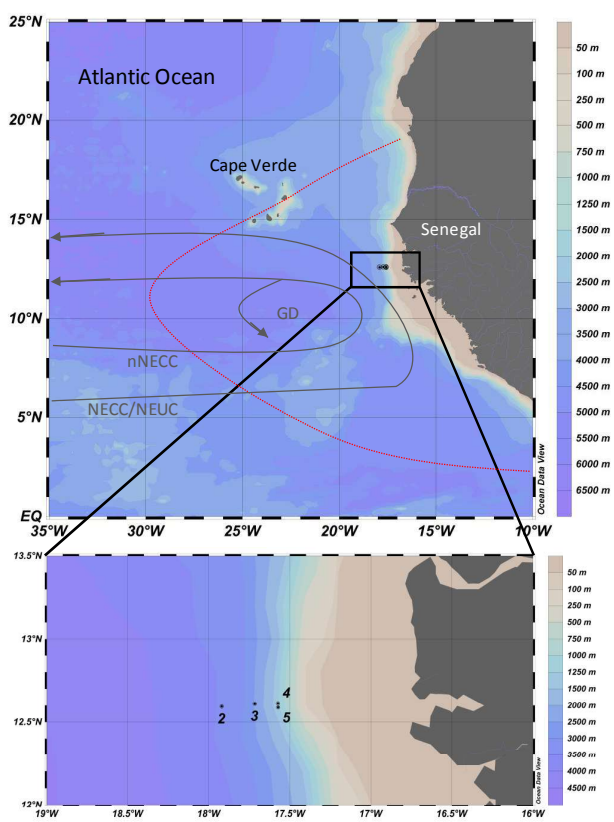


Figure 2

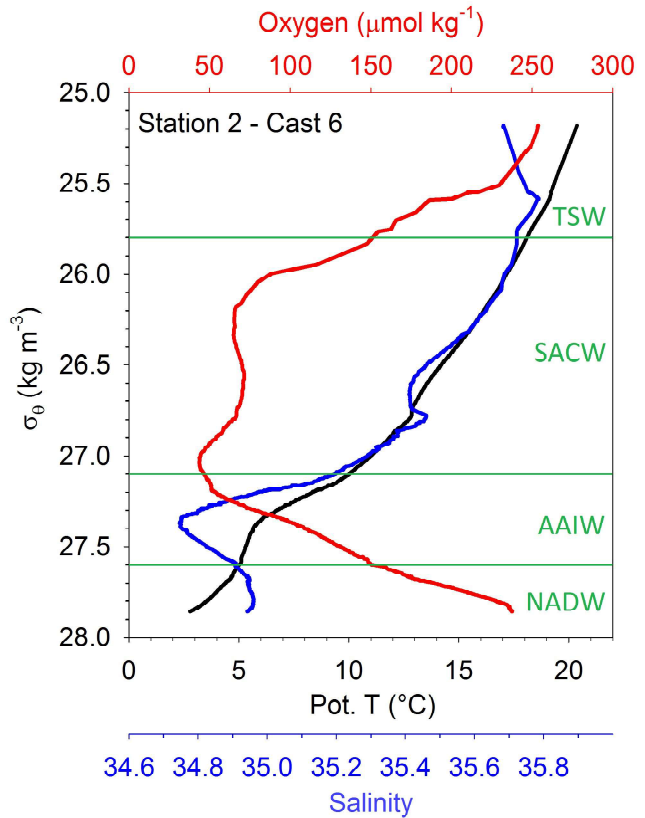
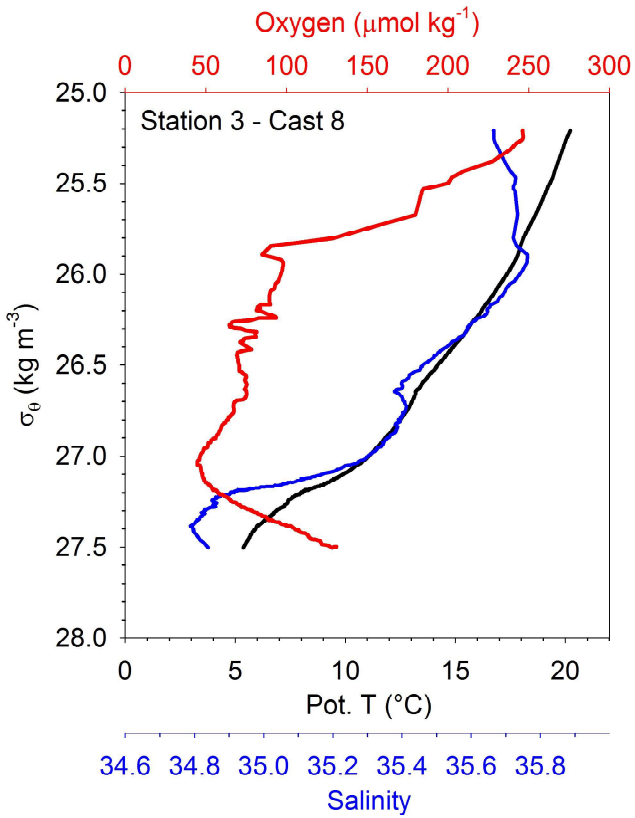
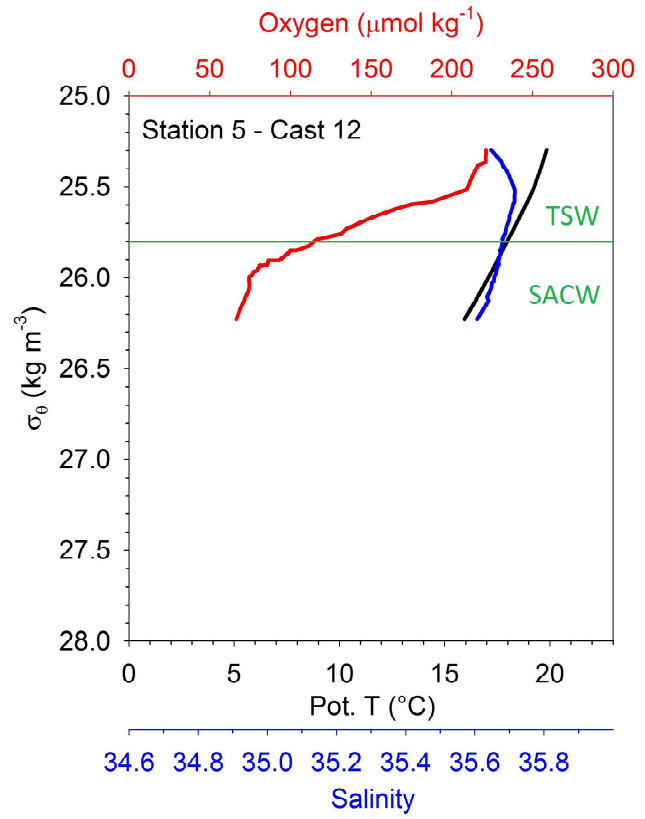
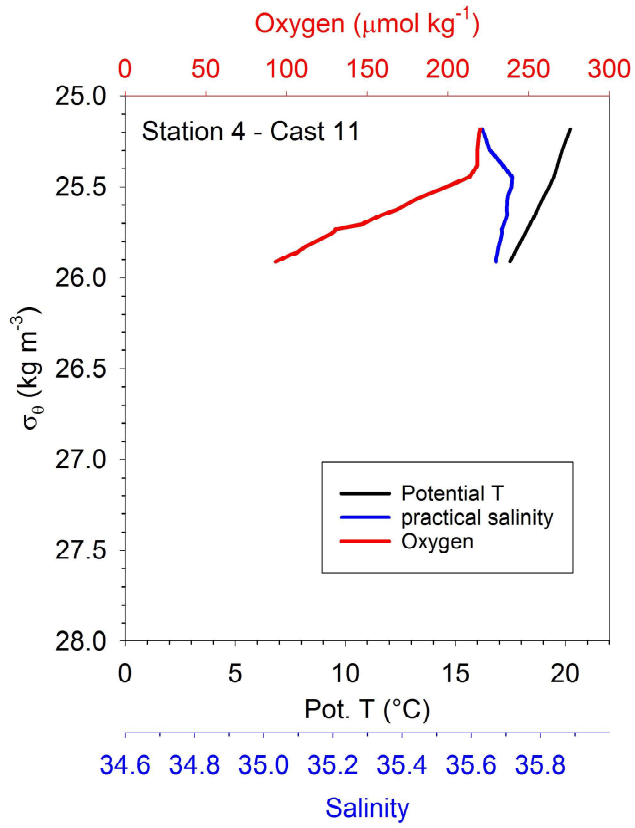


Figure 3

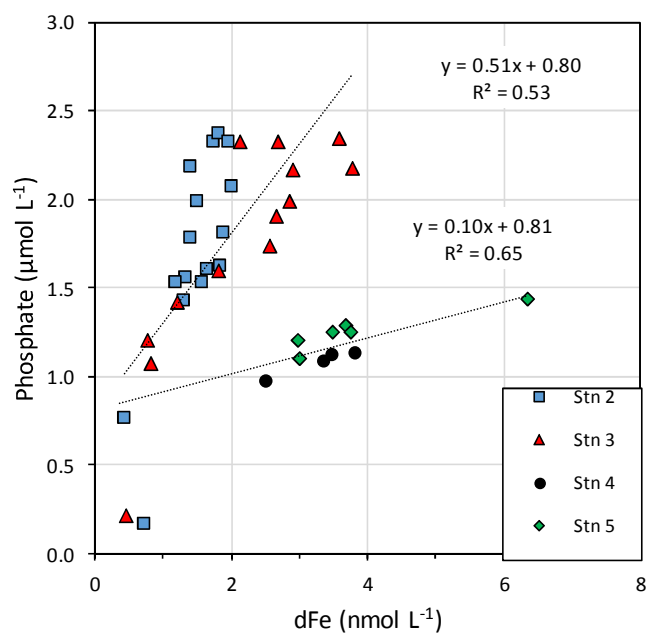


Figure 4

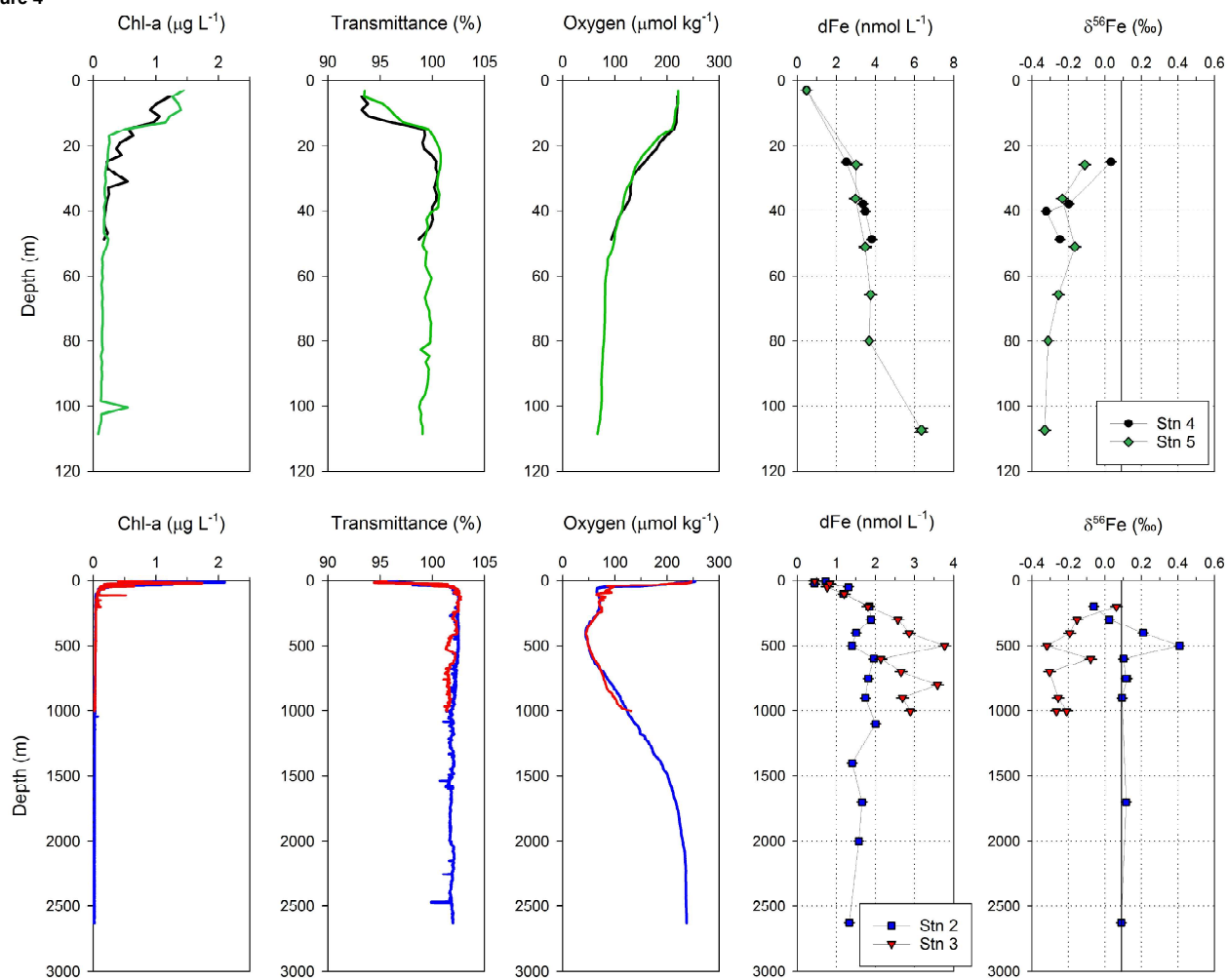


Figure 5

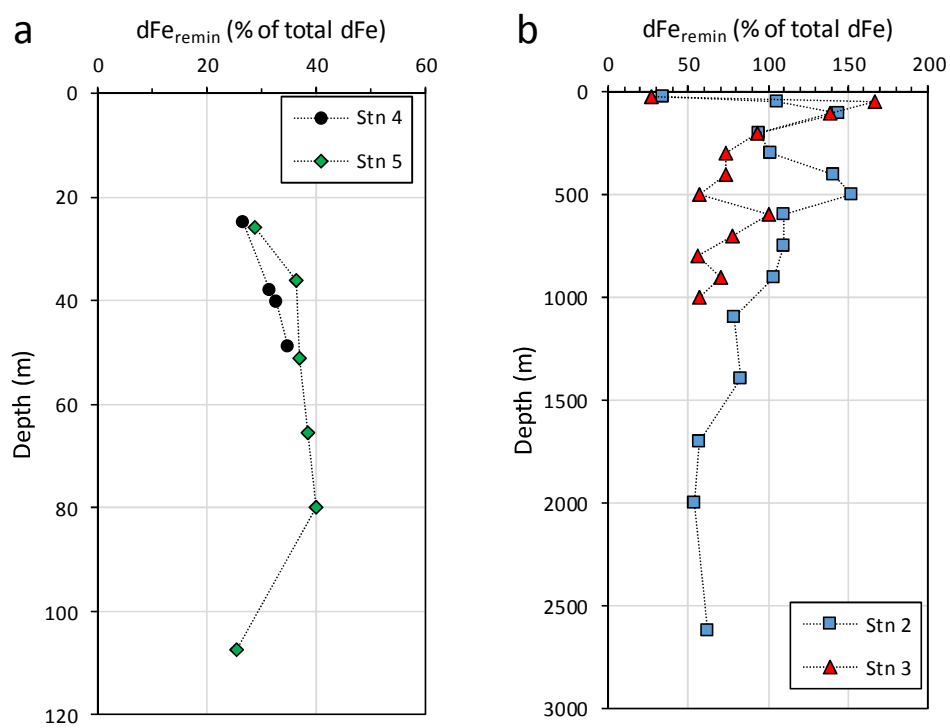


Figure 6

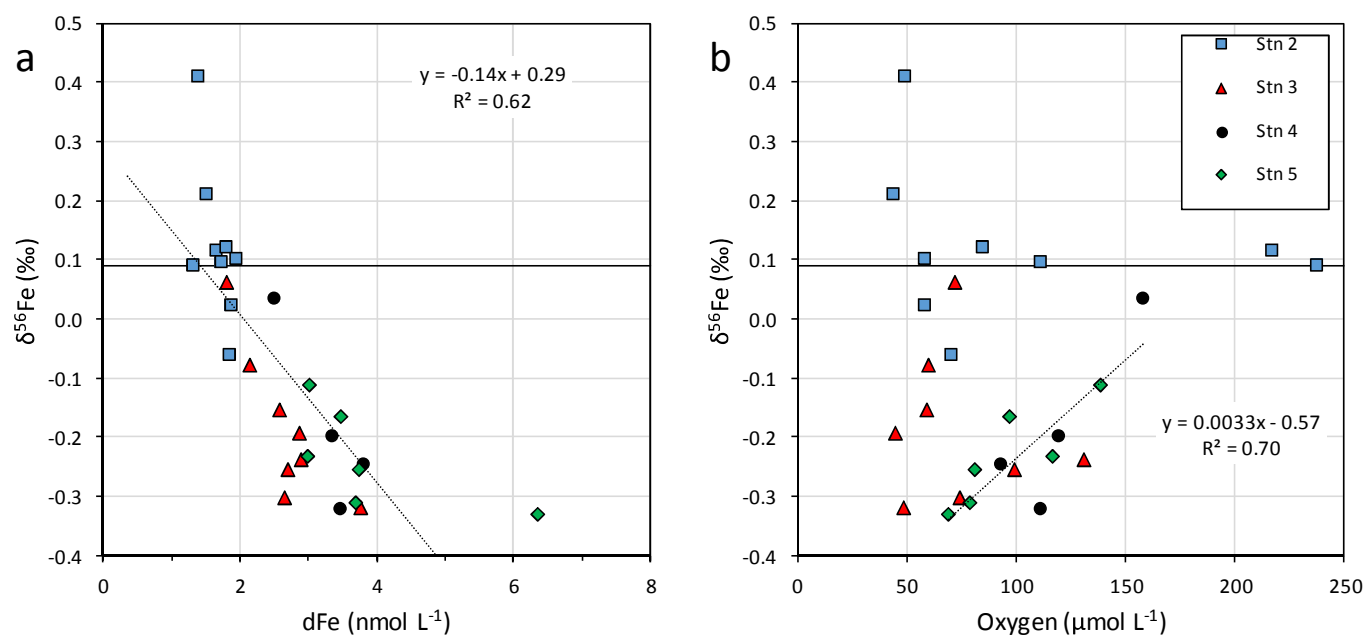


Figure 7

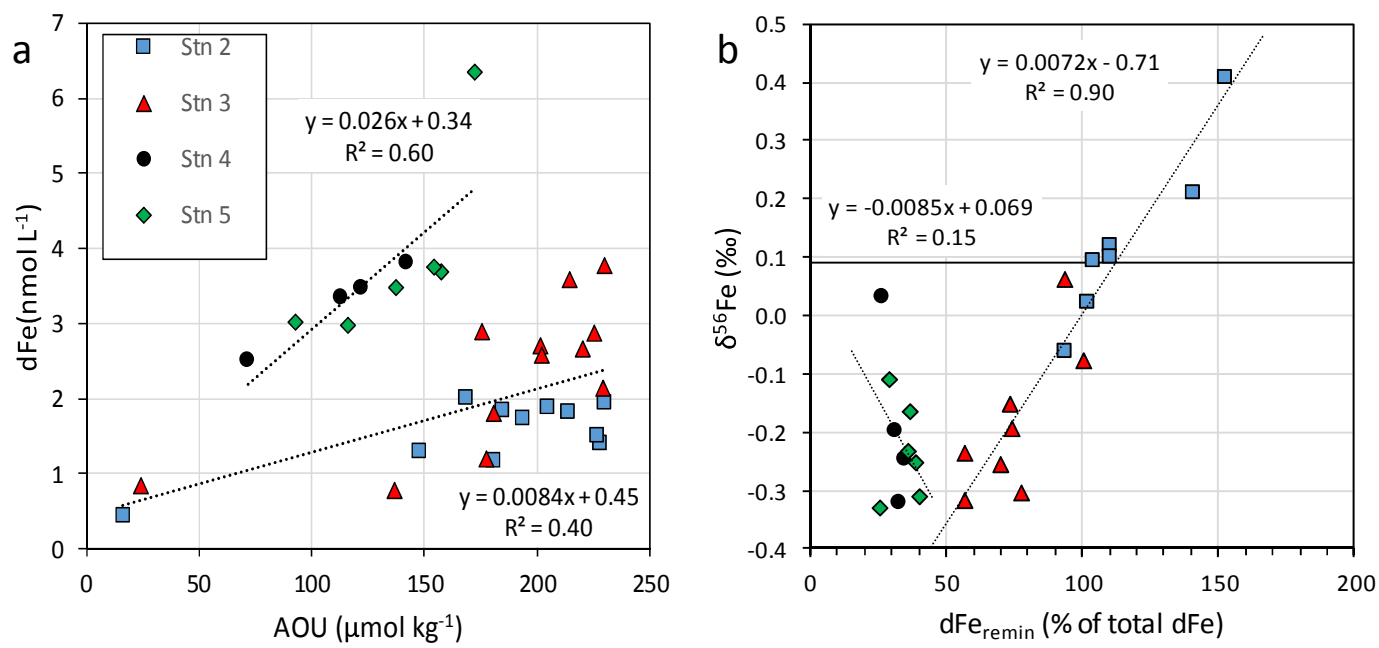


Figure 8

